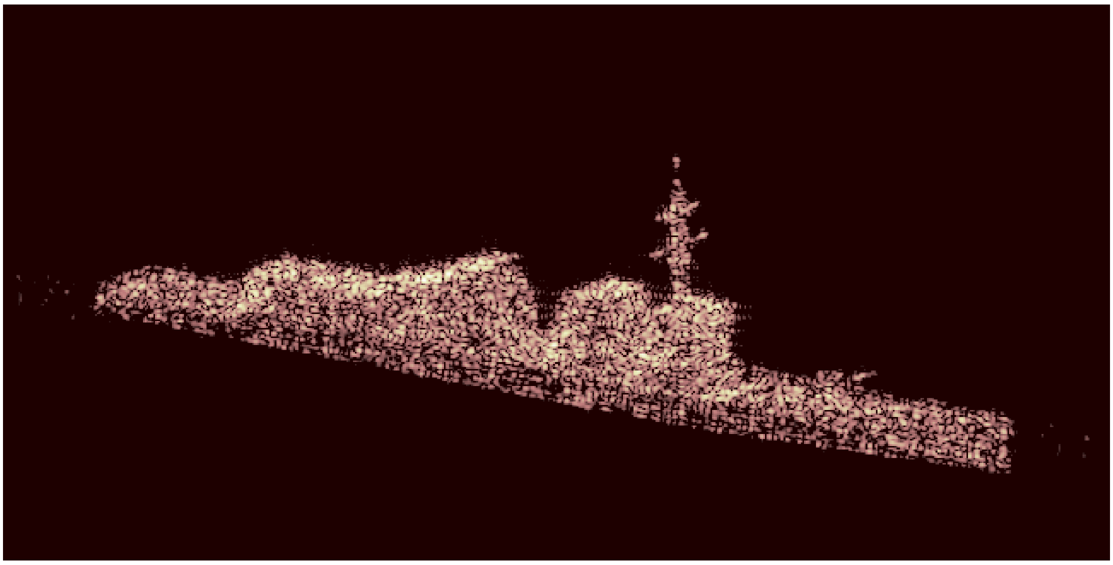

Maritime ISAR imaging with airborne radar

Master of Science Thesis

VERONICA BÄCKSTRÖM

ANTON SKÅRBRATT

Department of Radio and Space science
Radar Remote Sensing Group
CHALMERS UNIVERSITY OF TECHNOLOGY
Göteborg, Sweden, 2010

Maritime ISAR imaging with airborne radar
Master of Science Thesis
E. VERONICA BÄCKSTRÖM, K. ANTON SKÅRBRATT

Department of Radio and Space science
Radar Remote Sensing Group
Chalmers University of Technology
SE-412 96 Göteborg
Sweden
Telephone + 46 (0)31-772 1000

Cover:
Simulated ISAR image of a fictive destroyer, see pages 28-29 for further information.

Department of Radio and Space science
Göteborg, Sweden 2010

Abstract

Inverse synthetic aperture radar (ISAR) provides a way to produce high quality images of ships by use of their angular motion. This report addresses how this can be done and what possibilities, and difficulties, that are associated with the technique. Simulations have been conducted in Matlab consisting of 3D models of two ship types and their motion, as well as implementation of a signal processing algorithm for ISAR imaging. Various scenarios have been simulated to investigate the demands on performance to achieve images that can be used for identification. Results from these are presented for both full knowledge of the ship's motion and for estimations when this knowledge is absent. The simulated ship motions seem to provide enough resolution to recognize major ship features and the most suitable coherent processing time was found to be around one second for larger ships. Simulations also showed that a direct Fourier processing of the collected signal gives promising results for identification purposes.

Table of contents

List of abbreviations **1**

List of symbols **2**

1. Introduction **3**
- 1.1. Background 3
- 1.2. Purpose 3
- 1.3. Limitations 3

2. Theory **3**
- 2.1. ISAR 4
  - 2.1.1. Concept 4
  - 2.1.2. Geometry 6
  - 2.1.3. Sources of error 7
  - 2.1.4. Polar Format Algorithm 8
  - 2.1.5. Interpolation 13
- 2.2. Ship motion 14
  - 2.2.1. General 14
  - 2.2.2. Mathematical description 17

3. Simulations and Results **20**
- 3.1. Software overview and prerequisites 20
- 3.2. Initial algorithm tests 23
  - 3.2.1. Geometric distortion 24
  - 3.2.2. Signal strength degradation 24
  - 3.2.3. Resolution 24
- 3.3. Broadside profile 25
  - 3.3.1. Pure pitch 25
  - 3.3.2. Motion in three degrees of freedom 27
- 3.4. Dynamic IDP 28
- 3.5. Motion estimation 31
- 3.6. Changes in coherent processing time 35
- 3.7. Decreased roll motion 39

4. Conclusions **40**

5. Future work **41**

Acknowledgements **42**

List of abbreviations
in alphabetic order

APC	Antenna phase center
CPT	Coherent processing time
DFT	Discrete fourier transform
FFT	Fast fourier transform
FIA	Fixed incidence angle
FTP	Focus target plane
ISAR	Inverse synthetic aperture radar
PFA	Polar format algorithm
PRF	Pulse repetition frequency
QPE	Quadrature phase error
RCS	Radar cross section
RF	Radio frequency
SAR	Synthetic aperture radar
VPH	Video phase history

List of symbols

in order of appearance

ρ_a resolution in cross-range

$\Delta\theta$ the angle that a target is viewed through during the processing

λ_c center wavelength

ρ_r resolution in range

c speed of light

B bandwidth

$\boldsymbol{R}_a$ radar vector

θ_a squint angle

ϕ_{a} incidence angle

r_0 allowable scene radius for the polar format algorithm

$R_{\boldsymbol{ac}}$ distance between radar and scene center

$K_{\boldsymbol{a}}$ mainlobe-broadening factor

$\boldsymbol{R}_{\boldsymbol{t}}$ vector between radar and target

$\boldsymbol{K}_{\boldsymbol{a}}$ radar vector in K-space

$K_{\boldsymbol{x}}$ x-dimension in K-space

$K_{\boldsymbol{y}}$ y-dimension in K-space

$K_{\boldsymbol{z}}$ z-dimension in K-space

f stepped frequency

θ_p squint angle in K-space

ϕ_{p} incidence angle in K-space

Φ phase of the radar signal

S collected radar signal

K_U input grid vector

K_V input grid vector

W_U scene extent in U-direction

W_V scene extent in V-direction

ΔU pixel spacing in U-direction

ΔV pixel spacing in V-direction

T_r roll period

B_{beam} maximum beam at or below the water line

$\overline{GM}$ maximum metacentric height

T_p pitch constant

L length of ship

α yaw angle

β pitch angle

γ roll angle

$\boldsymbol{v}_{YAW}$ rotational vector for yaw

$\boldsymbol{v}_{ROLL}$ rotational vector for roll

$\boldsymbol{v}_{ROLL}$ rotational vector for roll

$\boldsymbol{R}_{YAW}$ rotational matrix for yaw

$\boldsymbol{R}_{PITCH}$ rotational matrix for pitch

$\boldsymbol{R}_{ROLL}$ rotational matrix for roll

$\boldsymbol{P}(0)$ starting location

$\boldsymbol{P}(\mathrm{t})$ location at time t

$\boldsymbol{P}_{trans}$ coordinate transformation matrix

ψ_y phase offset in yaw

ψ_p phase offset in pitch

ψ_r phase offset in roll

θ_g estimated angle span

θ_{true} true angle span

1. Introduction

1.1. Background

This report is a result of a master thesis conducted at Saab Electronic Defence Systems (EDS). EDS is a business unit within the Saab group that includes development and manufacturing of airborne and ground based surveillance radars. An area of interest within these technologies is a method to depict distant objects with high resolution. Inverse synthetic aperture radar (ISAR) is one way of accomplishing this. The main idea is to create an image using the phase difference that originates from the object's angular movement. More specifically, interest lie in being able to image ships based solely on their wave induced motions.

1.2. Purpose

Simulate and analyze ISAR images based on a developed model of ship motion together with an appropriate signal processing algorithm. The results aim to increase Saab's knowledge of airborne ISAR imaging and its applications.

1.3. Limitations

This thesis is purely theoretical and based on literature studies and simulations. No field trials have been made to evaluate to what extent the results corresponds to reality.

2. Theory

Synthetic aperture radar, or SAR, is a radar mapping technique for generating high resolution images of surface targets and terrain. The first experimental demonstration of such a mapping took place in 1953 when a section of Key West was generated by frequency analysis of data collected at around 10 GHz from a C-46 aircraft [2]. The concept was however brought to light already in 1951 by Carl Wiley of the Goodyear Aircraft Corporation [1]. The concept he proposed was given the name synthetic aperture radar to signify that a signal synthesis accomplished what would otherwise demand a larger antenna aperture than the one actually being used. "Synthetic aperture" in the name SAR refers to the distance that the radar travels during the time that reflectivity data is coherently integrated. The length of this synthetic aperture for a typical (side-looking) SAR system is the ground-track distance corresponding to this length. Implementation of this concept offers improvement in azimuth resolution and in most SAR systems comparable resolution in range is achieved by increasing the bandwidth of the transmitted pulse [1] [2].

The possibility of day and night operation in all weather combined with its fine two-dimensional resolution has made it possible for SAR to satisfy a variety of applications for both civilian and military users. Military SAR includes intelligence gathering, battlefield reconnaissance etc. and the civilian applications include topographic mapping, oil spill monitoring etc [1].

In this report inverse synthetic aperture radar (ISAR) is the technique used. ISAR is realizable when the object of interest is moving, which makes it possible to achieve the same large synthetic aperture as in SAR but without moving the radar platform, even though a movement of the platform might be present. When the object of interest rotates by a small amount it has the same effect as if the radar itself were to move a distance equal to the arc length at the range R from the object. ISAR applications include imaging of ships [3][4], aircrafts [5] and space objects as well as evaluating radar cross section of targets and target models [1][2].

2.1. ISAR

2.1.1. Concept

An image produced by ISAR is typically a two-dimensional mapping of the received signal energy. In case of sufficient resolution this means that the intensity of each individual pixel is the computed energy in the received signal from the corresponding location. The imaging process includes the following main steps [1]:

1. Generate, transmit and receive a wideband signal with a deterministic phase relationship between pulses.
2. Measure and compensate for the relative translational and rotational motion between the radar antenna phase center (APC) and the target.
3. Format the data based on radar system parameters and data collection geometry.
4. Compress the data in range and azimuth to achieve the desired resolution.

The signal processing for imaging scenes of moderate size and fine resolution is generally done by using the polar format algorithm (PFA), a subject that will be described in depth in section 2.1.4. With proper execution of steps 1 to 3 a two-dimensional fast Fourier transform (FFT) of the signal history data performs the data compression and finalizes the image [1]. The achieved resolution in cross-range dimension (for small angles of rotation) is defined as

$$\rho_a = \frac{\lambda_c}{2\Delta\theta} \tag{1}$$

where λ_c is the center wavelength and $\Delta\theta$ is the angle that the target is viewed through during the coherent processing time (CPT). The value of $\Delta\theta$ is typically no more than a few degrees in ISAR imaging with a minimum of around 2-3° required to obtain resolution of about 1 meter at S-band (wavelength = 10 cm) [7]. The image resolution in the range dimension is given by

$$\rho_r = \frac{c}{2B} \tag{2}$$

with B being the bandwidth and c the speed of light.

Throughout an ISAR imaging process it is common to use an image display plane (IDP). For optimal resolution this plane is defined by the radar line-of-sight and the direction of rotation of the target. The IDP then contains the line-of-sight vector and the vector cross product of the line-of-sight vector and the instantaneous angular velocity vector. In Figure 1 below the connection between the target motion and the projection plane is illustrated. Here the ship is illuminated by the radar from the bow and it is subject to a pure pitch counter-clockwise (CCW) motion which makes its angular velocity vector perpendicular to the page. This makes the vector cross product lie in the plane of the page in the vertical direction. If the ship were to pitch in the opposite direction (CW) the Doppler shift would also change direction and the image would be inverted [6].

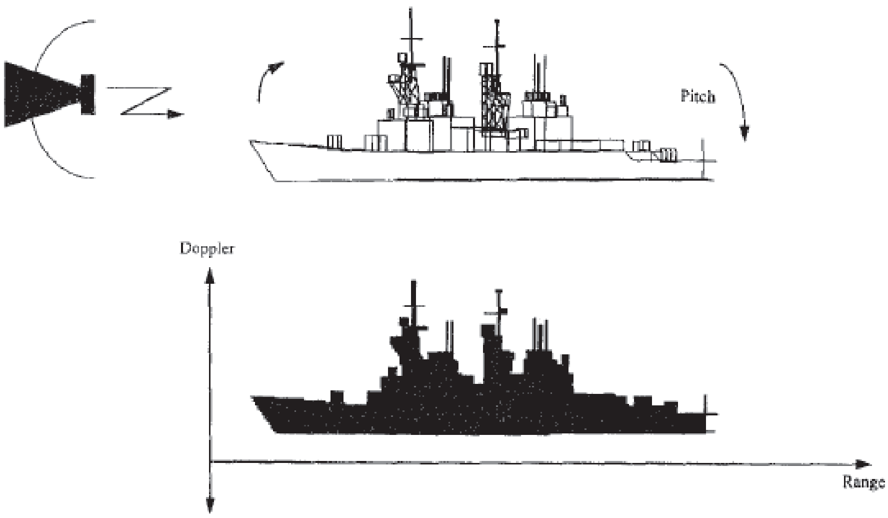

Figure 1: Illustration of the effect of a pure pitch motion and a radar looking straight towards the bow of the ship. Reproduced by permission from Musman, S. Kerr, D. Bachmann, C. , *Automatic recognition of ISAR ship images,* Aerospace and Electronic Systems, IEEE Transactions, Volume 32, Issue 4, Oct. 1996, © 1996 IEEE.

Roll motions, if the radar illumination aspect is other than parallel to the ship heading, give information about the vertical distribution of scatterers and yaw motions would give plan information. This dependence causes the ISAR image to vary considerably throughout a sequence of data collections. Generally an ISAR image can be expected to change significantly in 1 s, and radically within 5 s [6]. In Table 1, together with Figure 2, the ship image reproduction can be seen as a function of the ship motion and radar direction for several different scenarios.

Table 1: Ship image reproduction as a function of radar direction and ship motion, also see Figure 3. The vector between the antenna phase centre and scene centre is denoted r_c.

Direction of r_c	Ship rotation axis	Doppler resolution axis	Image perspective
$\hat{x}$ (forward)	$\hat{y}$ (pitch)	$\hat{z}$ (height)	Broadside profile
$\hat{x}$ (forward)	$\hat{z}$ (yaw)	$\hat{y}$ (transverse)	Plan view
$\hat{y}$ (broadside)	$\hat{x}$ (roll)	$\hat{z}$ (height)	Front profile
$\hat{y}$ (broadside)	$\hat{z}$ (yaw)	$\hat{x}$ (longitudinal)	Plan view
$\hat{z}$ (above)	$\hat{x}$ (roll)	$\hat{y}$ (transverse)	Front profile
$\hat{z}$ (above)	$\hat{y}$ (pitch)	$\hat{x}$ (longitudinal)	Broadside profile

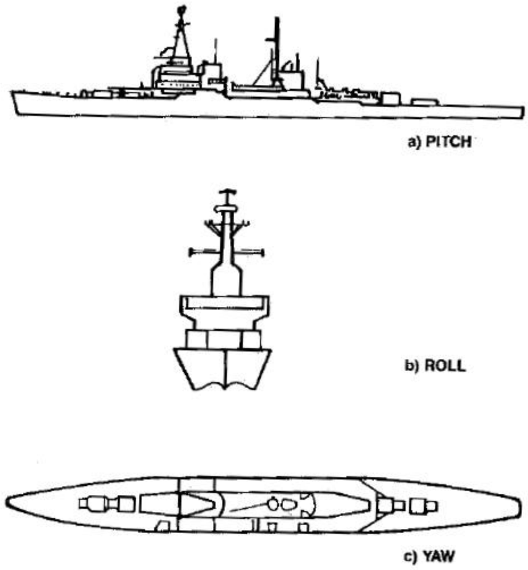

Figure 2: ISAR image views produced by a target with pure a) Pitch, b)Roll and c)Yaw motion. The radar lies anywhere in the plane of the paper, directed at the target. Reprocuced by permission from Donald R. Wehner, *High Resolution Radar*, Norwood, MA: Artech House, Inc., 1987 © 1987 by Artecth House, Inc.

2.1.2. Geometry

As mentioned earlier one can think of ISAR as if the target creates an apparent movement of the radar, see Figure 3, which in turn makes it possible to use the SAR approach.

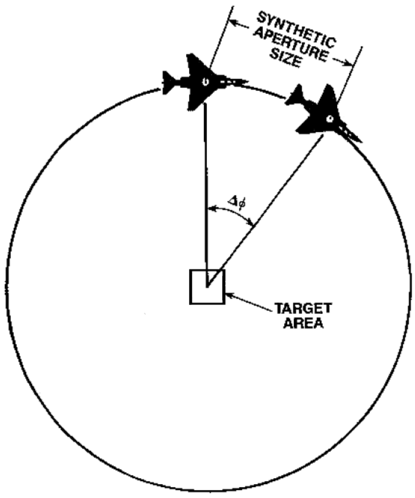

Figure 3: Illustration of the apparent motion of the radar when the target is rotating $\Delta\phi$. Reproduced by permission from Donald R. Wehner, *High Resolution Radar,* Norwood, MA: Artech House, Inc., 1987. © 1987 by Artech House, Inc.

In Figure 4 the concept of ISAR is shown in the form of the change mentioned above going from a maneuvering (translating, rotating) target to an equivalent stationary target. In this case the radar is fixed and the object of interest is a moving maritime target. Here changes in the target's velocity and attitude in the form of changes in roll, pitch and yaw contribute to an angular interval over which the radar sensor collects data. This means that the actual movement of the target determines the equivalent maneuvering flight path of the corresponding

SAR case. This way of modeling the data collection of an ISAR problem as an equivalent SAR case is common and will be used throughout this report.

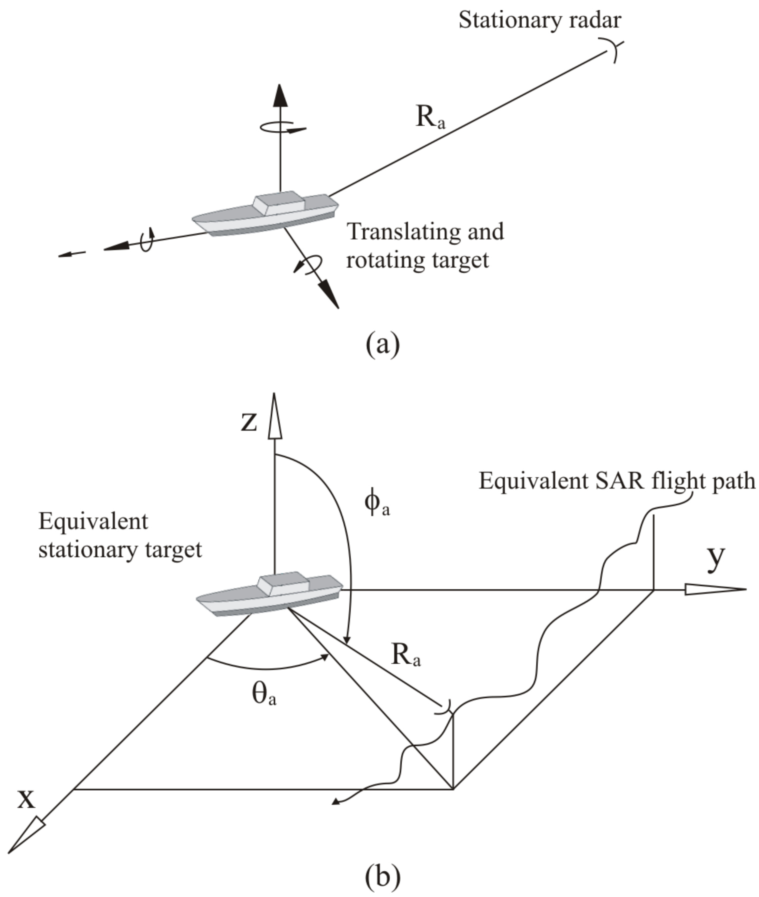

Figure 4: Concept and geometry. In a) a maneuvering (translating, rotating) target and the stationary radar is shown and in b) the equivalent stationary target and maneuvering SAR flight path is shown. Using this equivalent way of seeing it basically translates the ISAR problem to a SAR one.

Creating an analytical model using the equivalent SAR perspective demands that expressions for the quantities R_a, θ_a and ϕ_a are computed in terms of the motion of the ISAR target. Dominant contributors to θ_a and ϕ_a are likely to be attitude variations such as roll, pitch and yaw and R_a will only be affected by target translational motion. Since only relative motion is of importance this change is acceptable. This reversal makes all data collection, image planes, angles and all geometrical definitions apply equally to SAR and ISAR modeling.

2.1.3. Sources of error

Since ISAR imaging is a highly complex technique there are several sources of error [5]. Here is a list of some of them just to give a hint of the difficulties that are present during the process:

1. *Frequency and azimuth sampling errors:*
   If the frequency, or the changes in viewing angles, are incorrectly sampled it will result in aliased images which leads to spurious targets. The source

of this error is mainly unknown target or antenna motion, an aspect that will be investigated to a certain degree in this report.

2. *Integrated side lobe return:*
   Compression of range and azimuth data will cause image side lobes which will degrade the image quality. The combined power of all side lobes can smudge detail in low radar cross section (RCS) areas.
3. *Antenna aberrations:*
   There might be aberrations in the geometry result when the position of the antenna phase center changes with RF frequency or antenna aspect. This error source is not of interest in this report.
4. *Target dispersion and RCS:*
   The phase response of dispersive targets leads to it appearing to shift in position with RF frequency. Fluctuations in RCS amplitude may also cause distortions in the image. This error source is not of interest in this report.
5. *Multipath:*
   Multiple reflections can result in image distortions. This error source is not of interest in this report but for further information regarding this subject see [9].

2.1.4. Polar Format Algorithm

The work conducted in this section will follow a simplified and straightforward approach when investigating maritime ISAR using the polar format algorithm (PFA). Plane wave illumination is assumed to ease the algorithm development and place focus on investigation of how different ship motions affect image quality. Note however that in reality the spherical nature of the illuminated waves will have an impact on the phase response when imaging large ships.

Range curvature from the spherical waves introduces two sorts of image effects in the PFA. The first one is a geometric distortion[1] that can easily be corrected for with digital resampling in the processed image. The textbook [1] provides useful equations for correcting this kind of distortion in image domain. The second one is a scene size limiting defocus. An estimate for the allowable scene radius r_0 for the PFA when assuming $\pi/2$ allowance for the quadrature phase error (QPE) is [1]:

$$r_0 \leq \frac{2\rho_a}{K_a}\sqrt{\frac{R_{ac}}{\lambda_c}} \tag{3}$$

where R_{ac} is the distance between the radar and the scene center, ρ_a the azimuth resolution, K_a the generalized mainlobe-broadening factor and λ_c the center wavelength. In an airborne early warning and control system (AEW&C) relevant for this study a nearest imaging range can be set to R_{ac}=80 km together with a finest resolution of ρ_a=0.5 m. Also using a center frequency of 3.2 GHz and neglecting the mainlobe-broadening factor (K_a=1) will limit the scene to a radius

[1] This distortion arises from the fact that surfaces of constant range and surfaces of constant Doppler frequency fails to form an equally spaced orthogonal grid on a flat plane. For example, surfaces of constant range intersect the ground plane as circles while cones of constant Doppler intersect as hyperbolas [1].

of 922 m. It is reasonable to argue for a tougher QPE constraint of π/4 which results in a radius of 460 m.

The outer limit of maritime ISAR objects can be set to a Nimitz-class US aircraft carrier (333 m long). At the distance used above, it is still possible to image the aircraft carrier even when introducing a mainlobe broadening factor as well as lowering the resolution. This concludes the PFA to provide sufficient performance, and the simplification of using plane waves is acceptable.

PFA mainly operates in K-space and Figure 5 illustrates the basic data geometry both in data collection space and K-space. The target's motion is considered to trace an apparent radar flight path corresponding to the equivalent flight path in Figure 5(a) - in analogy with what is mentioned in section 2.1.2. Both the squint angle θ_a and incidence angle ϕ_a in the physical space are identical to θ_p and ϕ_p in K-space [1].

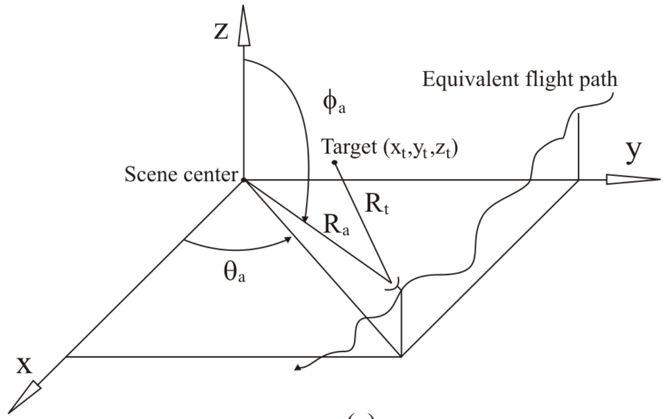

(a)

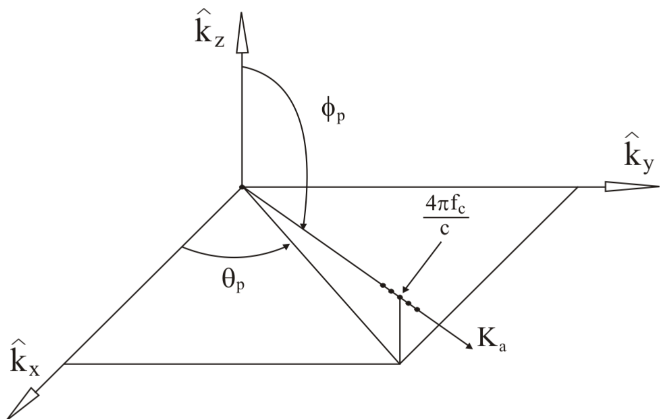

(b)

Figure 5: Illustration of the data collection geometry for an equivalent SAR case. (a) represents the actual geometry and (b) the corresponding data collection geometry in K-space.

First consider the case of a data collection in two dimensions where both the apparent radar vector $\boldsymbol{R_a}$ and rotational motion lies in the x-y plane. Assuming constant angular motion and a stepped frequency waveform, the resulting data collection grid in K-space will be the familiar polar grid seen in Figure 6.

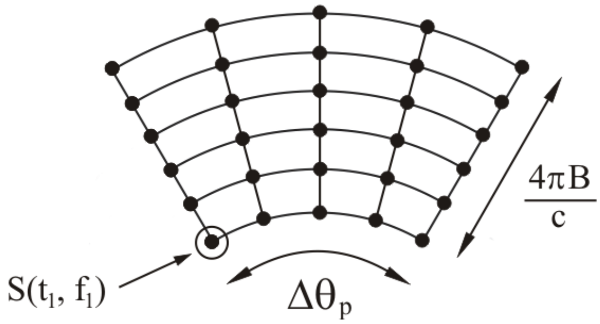

Figure 6: Data collection grid when the radar platform and rotation lie in the same plane. Here $S(t_1,f_1)$ is the collected signal for the first time sample and first frequency step, $\Delta\theta_p$ is the total angular displacement during coherent processing and B is the bandwidth.

ISAR imaging is sometimes more complex and the target's motion is usually in three dimensions. The resulting collection grid traced by the apparent radar vector $\boldsymbol{K}_a$ in K-space is then described by:

$$K_x = \frac{4\pi f}{c}\sin(\phi_p)\cos(\theta_p) \tag{4}$$

$$K_y = \frac{4\pi f}{c}\sin(\phi_p)\sin(\theta_p) \tag{5}$$

$$K_z = \frac{4\pi f}{c}\cos(\phi_p) \tag{6}$$

with stepped frequency f, squint angle θ_p, incidence angle ϕ_p and speed of light c as collection parameters. Figure 7 illustrates a three dimensional collection geometry with rotation around the z-axis and a fixed incidence angle. This specific case will produce a collection surface equivalent to a segment of a cone.

It is now time to state the equation for the received phase information of a single point scatterer. Assuming plane wave illumination and a stepped frequency waveform, the signal phase equation of a point scatterer becomes [10]:

$$\Phi(K_x, K_y, K_z) = \exp\left[j(x_t K_x + y_t K_y + z_t K_z)\right] \tag{7}$$

This expression can be identified as the integration kernel of a three dimensional Fourier transform[2]. Considering the target to consist of N point scatterers with different complex amplitude responses A_c, the collected signal will be a sum of their individual contributions at each time- and frequency sample, see (8). Note that θ_p and ϕ_p is changing with time in (4)-(6) as the target rotates, which will result in $K_{x,y,z}$ being a function of time and frequency.

$$S(t,f) = \sum_{n=1}^{N} A_c(n)\exp\left[j(x_t(n)K_x(t,f) + y_t(n)K_y(t,f) + z_t(n)K_z(t,f))\right] \tag{8}$$

[2] Depending on the sign convention it can also be seen as an inverse Fourier transform, but this will not affect the end result.

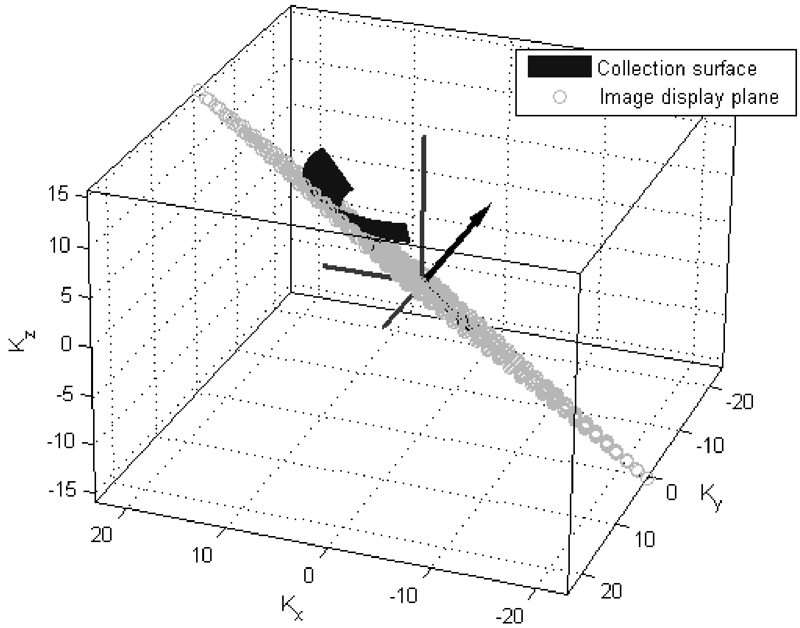

Figure 7: Illustration of ISAR data collection and image display plane at fixed incidence angle. The arrow seen represents the IDP normal vector.

General ISAR applications prefer a two dimensional image of the target, which makes it necessary to project the three dimensional K-vector onto a selected processing plane equivalent to the IDP. Note that the direction used to project the data defines where the scatterers will be focused. This is called the focus target plane (FTP). Using orthogonal projection will result in the FTP and the IDP to coincide, but this is not a necessary choice [10].

Now assume the data to lie in a projected grid in the IDP - see Figure 8 for illustration. An FFT transformation to the image room requires the data to lie in a rectangular grid. Creation of a new grid, and interpolation to it, is therefore a crucial step in the PFA.

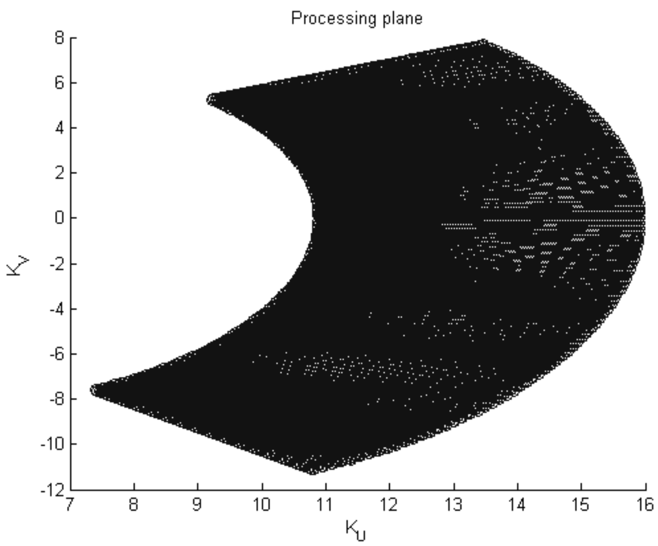

Figure 8: Example of a projected grid in K-space.

A suitable grid can be created from the input grid vectors K_U and K_V which are defined according to equations 9 and 10, where W_U & W_V and ΔU & ΔV is the scene extent and the pixel spacing in image plane.

$$K_U = -\frac{\pi}{W_U} : \frac{2\pi}{\Delta U} : \frac{\pi}{W_U} \tag{9}$$

$$K_V = -\frac{\pi}{W_V} : \frac{2\pi}{\Delta V} : \frac{\pi}{W_V} \tag{10}$$

What interpolation technique to use is depending on the original grid spacing. A sinc-filter is often mathematically the best choice, but since the interpolation step is the most time consuming it could be wise to chose e.g. a linear or nearest neighbor filter if the situation allows it. The final step is to transform the interpolated data to image space by using a two dimensional FFT.

Now consider a more general case were the motion is no longer bound to one fix axis. Any arbitrary rotation can be described by adding three types of rotation; a description in three degrees of freedom. If the target ship is crossing a sea with severe sea state, containing high wind velocities and significant wave amplitudes, it will unquestionably experience multi-axis rotation and hence a more complex imaging situation. Each one of the rotation axes will, alone, produce resolution in one dimension. How the resolution dimension (image perspective) is related to the ship's rotation axis and the radar direction can be seen in Table 1 in Section 2.2.

If motion exists in all three degrees of freedom it will give rise to the possibility of three-dimensional imaging. Still following the geometrical convention of assigning the radar an apparent motion as a result of the ship's rotation, the apparent radar vector $\boldsymbol{K_a}$ will trace an arc in the 3D K-space. Above it was illustrated that this arc has the form of a cone if motion exists around the z-axis only. If the rotation is generalized, e.g. around an arbitrary axis which is changing with time, $\boldsymbol{K_a}$ will trace a much more complex pattern according to:

$$K_a = \frac{4\pi f}{c}\left[\sin(\phi_p)\cos(\theta_p)\cdot\hat{k}_x + \sin(\phi_p)\sin(\theta_p)\cdot\hat{k}_y + \cos(\phi_p)\cdot\hat{k}_z\right] \tag{11}$$

To be able to image the target it is crucial to map the collected data to the correct position in K-space. One of the greatest challenges in maritime ISAR is therefore to estimate the motion of the target and trace the correct apparent radar path. Parts of the simulations, presented in section 3, investigate how errors in the motion estimation affect the image quality.

Assuming the data to be distributed in K-space sufficiently close to their true positions, it is now time to choose a proper IDP. This choice is also highly dependent on how the target's rotation is estimated and its relative orientation. For example, if the ship is experiencing a dominant pitch motion and oriented to move towards the radar, it would be wise to choose an IDP that coincides with a broadside profile – again see Table 1 if needed.

Choice of IDP could be done in a variety of ways:

- Manually by an operator.
- Automatically by iteration and image analysis algorithm.
- The IDP normal vector follows the radar line of sight vector with a squint angle offset of 90° for maximum resolution in height.

Projection of the data collection surface onto the IDP can be done in any direction suitable. Evaluating consequences from the choice of projection direction is beyond the scope of this paper and projection is done orthogonally throughout the simulations, remembering that this results in FTP and IDP to coincide.

To summarize, an ISAR image of a rotating ship can be, and is in this report, produced in the following way:

1. Collect the VPH data and place it in K-space corresponding to the surface traced by the apparent radar vector $\boldsymbol{r}_c$.
2. Project the surface orthogonally onto a selected IDP.
3. Create a rectangular grid in the IDP.
4. Interpolate the projected data to the rectangular grid.
5. Perform a two dimensional FFT on the interpolated data to produce an image of the target.

2.1.5. Interpolation

This subsection will briefly discuss different interpolation techniques that are relevant to use when interpolating between the polar- and rectangular grids. Focus will not lie on explaining details of how to create such interpolators, but rather discuss different approaches from an overall perspective. The most important parameters are resolution and speed.

Polar formatting creates the situation of having to interpolate in two dimensions – range and cross-range. This can be done either with a single two-dimensional filter or using two one-dimensional filters. The former has a processing time proportional to the filter length squared, while the latter is faster with a processing time proportional to twice the filter length [1]. Interpolating in two steps employs two different cases:

- Range interpolation is performed from uniform input samples to uniform output samples.
- Cross-range interpolation is performed from non-uniform input samples to uniform output samples.

A sinc interpolator is probably the best choice if the polar grid is sparsely sampled and [1] provides a detailed explanation on how to create such a filter. The situation is however more complex in azimuth direction since the samples are non-uniform. Standard sinc filters are built from the fact that the input spacing is uniform and monotonic, but maritime ISAR will in some cases produce the exact opposite – non-uniform samples which are not monotonic.

Upsampling of the azimuth spacing before interpolation to the uniform output grid could be done by zero-padding in Fourier space. An FFT can not be used since the input samples are non-uniform, which results in the use of a much slower DFT-core.

A non-realistic, but comfortable, way to create a perfect upsampling is simply by creating more cross-range samples in the radar simulator than allowed by the pulse repetition frequency (PRF). This is not an option in real operation, but could ease the algorithm development at this early stage in the study of maritime ISAR. After all, focus should lie on what image quality that can be produced by ship motion, not creating an optimal interpolator for misfortunate data collection.

When the input grid is, after upsampling, densely sampled compared to the output the following interpolation filters are considered here:

- Triangle-based 2D cubic interpolation using Matlab's griddata.
- Triangle-based 2D linear interpolation using Matlab's griddata.
- Nearest neighbor 2D interpolation using Matlab's griddata.

Matlab's griddata is especially constructed to interpolate from non-uniformly spaced matrices and therefore fits the purpose well [11].

2.2. Ship motion

As mentioned earlier a clear understanding of the motion of the object is crucial to be able to use ISAR for creating high resolution images. This section aims to give some theoretical background about the principles of ship motion and to discuss some limitations. Here you will also be able to read about coordinate systems and rotation matrices later used in the simulations.

2.2.1. General

In naval architecture one usually speaks of six degrees of freedom associated with six types of oscillatory motions. These are roll, pitch, yaw, surge, sway and heave [12]. In Figure 9 all of them are illustrated. Additional motions that are non oscillatory are heel, list, and trim [12] but those will not be considered in this report.

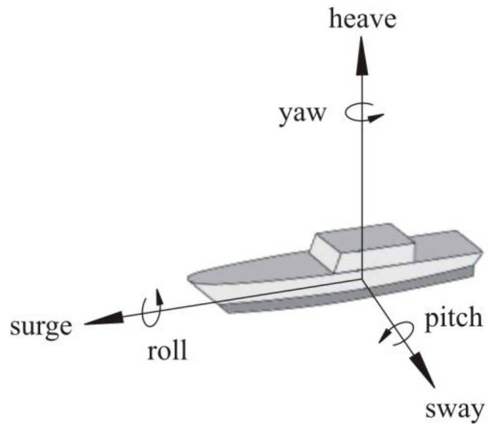

Figure 9: Definitions of ship oscillatory motion.

A ship will be regarded as a rigid body, which is not entirely true since it will most likely bend, stretch and twist to some extent [12]. This limitation is done with the assumption that the effects of these deformations on image quality will be small in comparison to the increased complexity that they bring to the calculations.

The complex motion of a ship will in general include the oscillatory motions of roll, pitch and yaw. These motions can be considered as rotational vectors which can be added to create a net instantaneous rotational axis. This axis will change in magnitude and direction for different points in time due to the various angular oscillations [12].

Roll, pitch and yaw are induced by waves in the sea surface and the nature of these waves is typically described in terms of sea-state, a quantity that can be characterized depending on wind speed and wave height according to Table 2. Motions originating from sea waves tend to be of sinusoidal character and the most significant ones of the above mentioned are roll and pitch [12]. Among these two roll is normally the least damped, resulting in that the roll angle can be relatively large in magnitude. Pitch on the other hand can behave in a very nonlinear way in heavy sea states because the bow tends to elevate out of the water and slam the water surface on return. When it comes to sway, surge, and heave they are typically heavily damped [12]. With this in mind the most preeminent motions concerning ISAR imaging are roll, pitch and yaw and therefore focus will lie on those three. All others will be assumed to have zero contribution.

Table 2: Sea states in the open sea, North Atlantic [13].

Sea state	Significant wave height [m]	Sustained wind speed [knots]	Percent probability	Modal wave period range [s]	Modal wave period most probable [s]
0-1	0-0.1	0-6	0.70	-	-
2	0.1-0.5	7-10	6.80	3-15	7
3	0.5-1.25	11-16	23.70	5-15.5	8
4	1.25-2.5	17-21	27.80	6-16	9
5	2.5-4.0	22-27	20.64	7-16.5	10
6	4.0-6.0	28-47	13.15	9-17	12
7	6.0-9.0	48-55	6.05	10-18	14
8	9.0-14.0	56-63	1.11	13-19	17
>8	>14.0	>63	0.05	18-24	20

Roll

Typical roll angles depend on sea state and for sea state 4 it may be single digit degrees for certain roll suppressing designs. In sea state 8 it can be up to several tens of degrees [12]. These angles depend not only on the sea waves but also how well the wave energy couples with the hull. The roll period can be calculated from the following empirical formula [12]:

$$T_r = \frac{CB_{beam}}{\sqrt{\overline{GM}}} \tag{12}$$

where C is the roll constant, typically between 0.69 and 0.89 $s/\sqrt{m}$ for large ships, based on experimental results from similar ships. B_{beam} is the maximum beam at or below the water line, and $\overline{GM}$ is the maximum metacentric height (see Figure 10), usually low-single-digit meters. Typical roll periods are about 10 to 20 seconds [12].

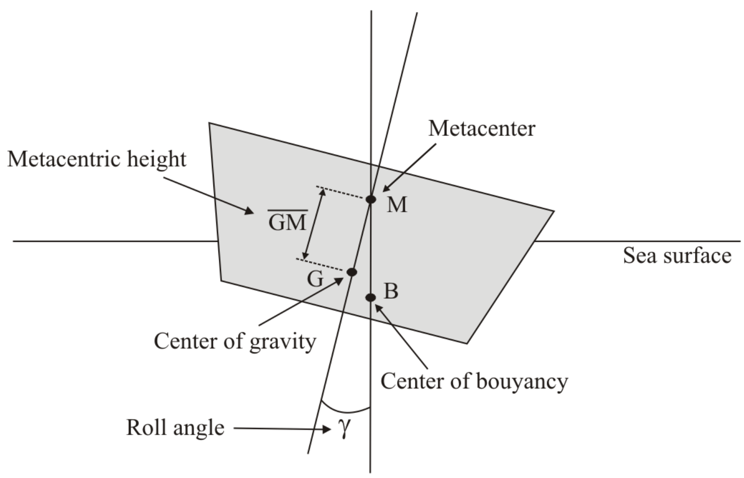

Figure 10: Description of metacentric height. For further information regarding the definitions used in this picture, see [12].

Pitch

The maximum pitch angle depends on sea state and ship length, a longer ship allows less pitch angle. Typical values for pitch angle are 1-2 degrees in sea state 4 and up to 5-11 degrees in sea state 8 depending on how long the ship is. In Table 3 typical values for pitch periods can be seen. The values in this table can be fitted to a curve described by the following expression [12]:

$$T_p = 2.44 + 0.032\,L - 0.00036\,L^2 \tag{13}$$

where T_p is the pitch period and L is the length of the ship in meters.

Table 3: Typical values of pitch periods as a function of ship length [12].

Length of ship [m]	Pitch period [s]
<46	3.5
46-76	4
76-107	5
107-152	6
152-213	7
>213	8

Yaw

Yaw is an effect of temporary bearing changes and is typically damped by rudder control. The time period for yaw is generally equal to the wave period [12].

2.2.2. Mathematical description

The coordinate system xyz used in this section has its origin fixed in the center of gravity and is translating with the ship. This choice of reference allows the ship's rotational motion to be described in the following way [14]:

1. Counterclockwise rotation about the z-axis by the yaw angle α(t).
2. Counterclockwise rotation about the new (once rotated) y-axis by the pitch angle β(t).
3. Counterclockwise rotation about the new (twice rotated) x-axis by the roll angle γ(t).

In words, this results in the ship's yaw-axis being fixed to the z-axis, pointing opposite the direction of gravity. The pitch axis is on the other hand bound to the boats pointing direction and the roll axis is totally fixed to the ship's physical layout and is therefore rotated by both the preceding yaw and pitch motion – see Figure 11.

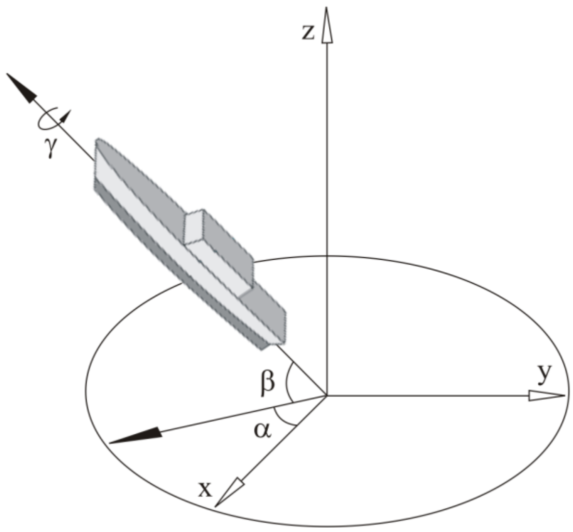

Figure 11: Illustration of the rotational motion of a ship with yaw angle α, pitch angle β and roll angle γ.

One way of mathematically describing this motion is by defining rotation around a line described by the vector v in the following way [15]:

$$v_{YAW}(t) = (0,0,1)^T \quad \rightarrow \text{Rotational matrix } R_{YAW}(t). \tag{14}$$

$$v_{PITCH}(t) = R_{YAW}(t)(0,1,0)^T \quad \rightarrow \text{Rotational matrix } R_{PITCH}(t). \tag{15}$$

$$v_{ROLL}(t) = R_{PITCH}(t)R_{YAW}(t)(1,0,0)^T \quad \rightarrow \text{Rotational matrix } R_{ROLL}(t). \tag{16}$$

The point ***P***'s new location at time sample t is calculated from its starting coordinates $\boldsymbol{P}(0)=(x_0, y_0, z_0)^T$ in the following way:

$$P(t) = R_{ROLL}(t)R_{PITCH}(t)R_{YAW}(t)P(0) \tag{17}$$

The corresponding rotation matrices are calculated by the means of coordinate transformations, where the line of rotation is defined by the vector $\boldsymbol{v} = (a, b, c)^T$ as above. All points are transformed from stationary xyz-space (translating with the boat) to a new space $(\bar{x}, \bar{y}, \bar{z})$, where the $\bar{z}$ -axis has the same direction as $\boldsymbol{v}$ - see Figure 12 [15].

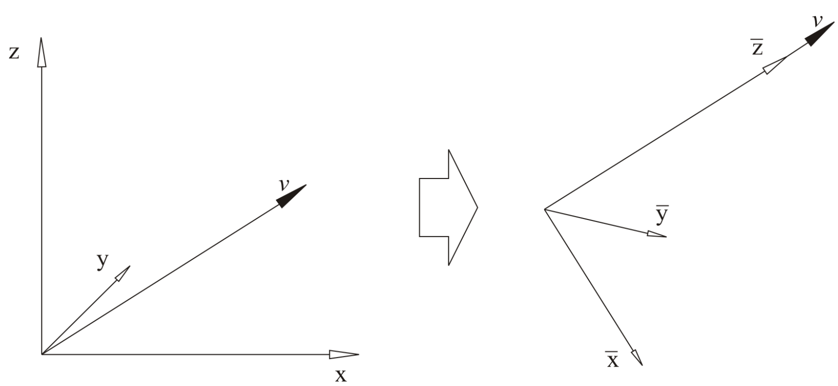

Figure 12: Coordinate transformation to align the z-axis with the line of rotation *v*.

This is done with the coordinate transformation matrix $\boldsymbol{P}_{trans}$, which is constructed in the following way [15]: [3]

$$P_{trans} = \left[\bar{e}_x, \bar{e}_y, \bar{e}_z\right] = \begin{bmatrix} p_{11} & p_{12} & p_{13} \\ p_{21} & p_{22} & p_{23} \\ p_{31} & p_{32} & p_{33} \end{bmatrix} \text{ where} \tag{18}$$

$$\bar{e}_z = \frac{1}{|v|} v = \begin{bmatrix} p_{13} \\ p_{23} \\ p_{33} \end{bmatrix} = \frac{1}{\sqrt{a^2 + b^2 + c^2}} \begin{bmatrix} a \\ b \\ c \end{bmatrix} \tag{19}$$

$$\bar{e}_y = \begin{bmatrix} p_{12} \\ p_{22} \\ p_{32} \end{bmatrix} = \frac{1}{\sqrt{a^2 + b^2}} \begin{bmatrix} -b \\ a \\ 0 \end{bmatrix} \tag{20}$$

$$\bar{e}_x = \begin{bmatrix} p_{11} \\ p_{21} \\ p_{31} \end{bmatrix} = \bar{e}_y \times \bar{e}_z \tag{21}$$

and rotation around z-axis is defined as

$$R_z(\alpha) = \begin{bmatrix} \cos\alpha & -\sin\alpha & 0 \\ \sin\alpha & \cos\alpha & 0 \\ 0 & 0 & 1 \end{bmatrix} \tag{22}$$

Since the coordinate transformation places the new $\bar{z}$ -axis in the same direction as $\boldsymbol{v}$, the rotation matrix $\boldsymbol{R}$ can be written as

$$R = P_{trans} R_z(\alpha) P_{trans}^T \tag{23}$$

with rotation of angle α around the line $\boldsymbol{v}$. Note that for calculation of yaw, pitch and roll matrices one simply replace the rotation angle α with $\alpha(t)$, $\beta(t)$ and $\gamma(t)$ and directional vector $\boldsymbol{v}$ with $\boldsymbol{v}_{Yaw}(t)$, $\boldsymbol{v}_{Pitch}(t)$ and $\boldsymbol{v}_{Roll}(t)$ respectively.

[3] Note that if the directional vector $v=(0,0,1)^T$ (as in the case of the yaw rotation) the coordinate transformation is unnecessary. This comes from the fact that the z-axis already points in the same direction as v and the equations are not defined for this specific case (division by 0 in $\bar{e}_y$).

3. Simulations and Results

3.1. *Software overview and prerequisites*

The work in this project has been done using Matlab and Figure 13 presents a flowchart of the developed software later used in the simulations.

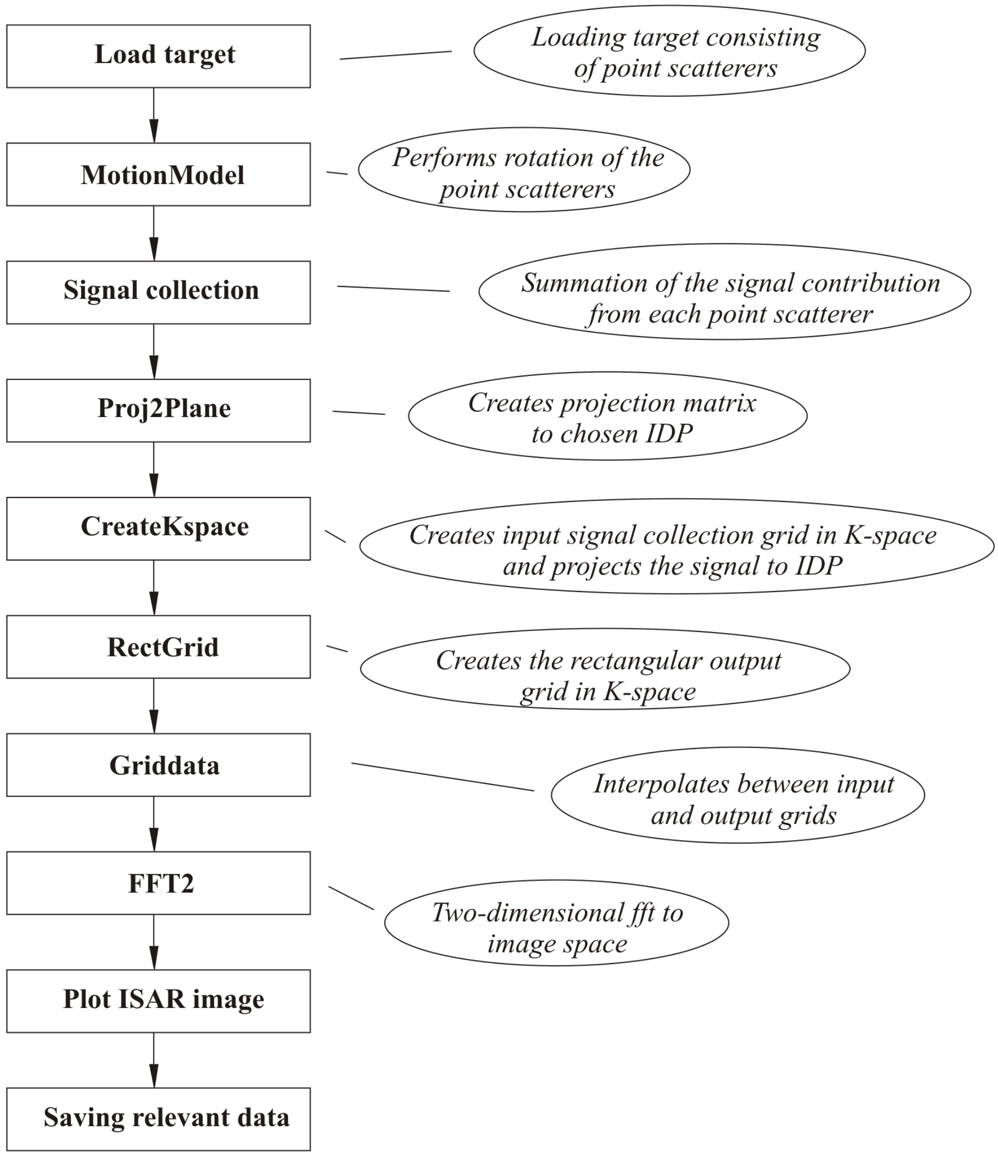

Figure 13: Flowchart over developed and built in Matlab software functions.

Matlab has also been used to build 3D models of a fishing boat and a destroyer. These models consist of numerous point scatterers approximately spaced by 1 m and have been carefully modeled to be as representative as possible for their specific type of ship. The choice of spacing took into consideration the expected resolution constraints as well as demands on calculation speed. See Figure 14 and Figure 15 for an illustration of the fishing boat and destroyer models respectively. Note that the target models do not take shadowing under consideration, resulting in the fact that all point scatterers will return echoes at all times. This is a simplification of reality.

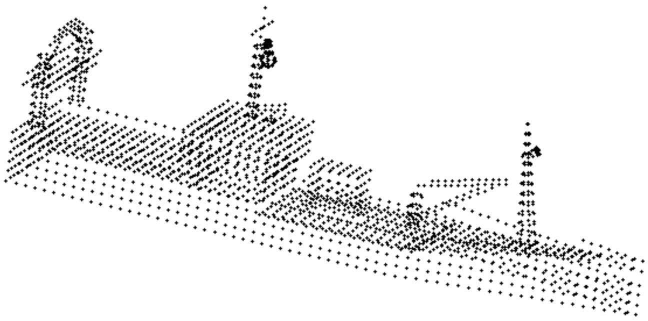

Figure 14: Illustration of the fishing boat model used in the simulations. The boat is constructed of point scatterers spaced by approximately 1 m. As inspiration for this model an ordinary fishing boat has been used giving a ship size of about 56 m in length and 12 m in width.

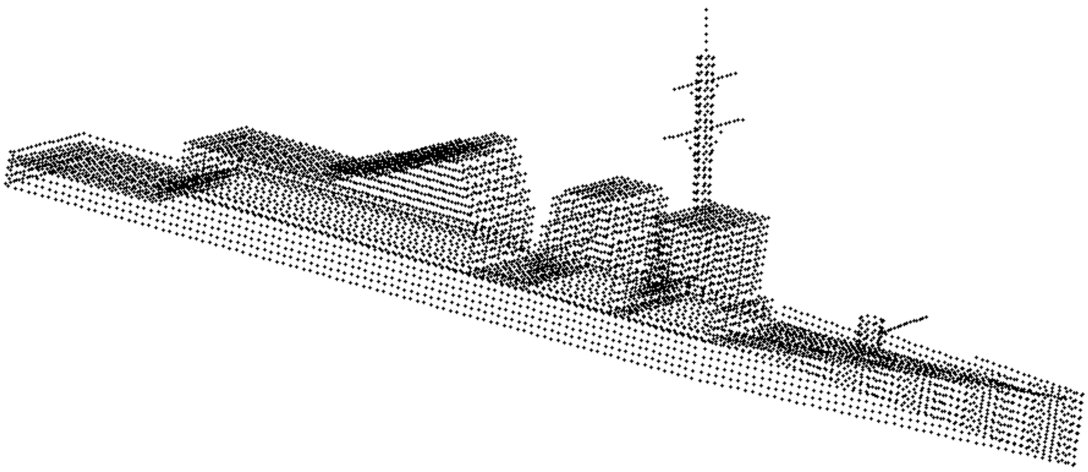

Figure 15: Illustration of the destroyer model used in the simulations. The ship is constructed of point scatterers spaced by approximately 1 m. As inspiration for this model a typical destroyer has been used giving a ship size of about 154 m in length and 18 m in width.

To make the simulations as realistic as possible a great deal of thought has been spent on the values used for the various parameters implemented in the software. Center frequency and bandwidth have for example been given values that are likely to be used in an airborne surveillance radar. The PRF however has been assigned twice its realistic value to ease interpolation. Values concerning the motion of the ships have been compiled in close contact with naval expertise at Chalmers University of Technology. Amplitudes and periods are set to represent a typical motion while crossing the most probable sea state (4) in the North Atlantic (see Table 2 for details). Harmonic motion will be assumed and therefore the following expressions are implemented:

$$\alpha(t) = A_y \sin(\frac{2\pi \cdot t}{T_y} + \psi_y) \tag{24}$$

$$\beta(t) = A_p \sin(\frac{2\pi \cdot t}{T_p} + \psi_p) \tag{25}$$

$$\gamma(t) = A_r \sin(\frac{2\pi \cdot t}{T_r} + \psi_r) \tag{26}$$

with $\alpha(t)$, $\beta(t)$ and $\gamma(t)$ being the angular displacement in yaw, pitch and roll respectively. $A_{y,p,r}$ is the corresponding amplitudes, $T_{y,p,r}$ the periods and $\psi_{y,p,r}$ the phase offsets.

The CPT used for the destroyer is set to 1 s and this value is cut in half for the fishing boat as a result of its relative angular motion. The incident angle has been calculated taking into consideration the typical flying height of an airborne surveillance system and the shortest possible detection range resulting in an angle of about 85.5°. The squint angle is initially set to 0° meaning that the radar is placed straight ahead of the ship.

In Table 4 a list of default values for the various parameters used in the simulations are shown. If nothing else is specifically indicated for each simulation, these are the values that are implemented. Finally, the complex amplitude response A_c for each point scatterer is set to be a two-dimensional Gaussian distribution and non-fluctuating in time. The amplitude response is related to RCS according to (27).

$$RCS \propto |A_c|^2 \tag{27}$$

Table 4: Default values for simulation parameters. If nothing else is specified these are the values used in each simulation.

Parameter	Value		Description
	Fishing boat	*Destroyer*	
f_c	3.2 GHz	3.2 GHz	Center frequency
B	200 MHz	200 MHz	Bandwidth
PRF	600 Hz	600 Hz	Pulse repetition frequency
N_f	250	250	Number of frequency samples
T_y	9 s	9 s	Yaw period
T_p	4 s	7 s	Pitch period
T_r	10 s	20 s	Roll period
A_y	2°	2°	Yaw amplitude
A_p	4°	2°	Pitch amplitude
A_r	15°	15°	Roll amplitude
T_{ill}	0.5 s	1 s	Coherent processing time
ϕ_a	85.5°	85.5°	Incidence angle
θ_a	0°	0°	Squint angle
interp	Cubic	Cubic	Interpolation technique
IDP	[90°, 90°, 1]	[90°, 90°, 1]	Normal vector to define IDP according to standard spherical coordinate system

Further on some additional limitations regarding the system has been implemented:

- Motion of the airborne radar relative to the scene center is not considered – perfect motion compensation is assumed.
- No efforts will be made to account for antenna contributions (beam-shape etc.).
- Adequate clutter suppression will be assumed.
- All point scatterers will return echoes at all times – no shadowing is included.

All the simulated results presented in sections 3.3 to 3.7 have been conducted in the form of videos of about 20 seconds in length. This makes it possible to visualize the imaging effects for different instances of CPT in the harmonic motion and eases the analyzing step. For obvious reasons all these images will not be presented in this report, merely a few representative ones will be displayed and analyzed.

3.2. Initial algorithm tests

To be able to properly analyze ISAR images of the simulated ships it is important to first understand the performance of the algorithm. This section therefore aims to investigate and evaluate a few characteristics of our implementation of the PFA.

All input parameters are set to represent the case of imaging a fishing boat with the exception of an incidence angle of 90° instead of 85.5° (to ease analysis of geometric distortion). The motion of the point scatterers have also been set to be a pure pitch motion, a justified choice since it is the only motion giving resolution in this scenario. The simulation specific parameters are given below and the reader is referred to section 3.1 and Table 4 for a full parametric list.

$\phi_a = 90°$
$A_y = 0$
$A_r = 0$

Figure 16 presents the ISAR image of seven point scatters located in the xz-plane and having a pure pitch motion. Their coordinates in space were (0,0,0), (30,0,0), (60,0,0), (0,0,30), (0,0,60), (30,0,30) and (60,0,60) and three properties were investigated: geometric distortion, signal strength degradation and resolution.

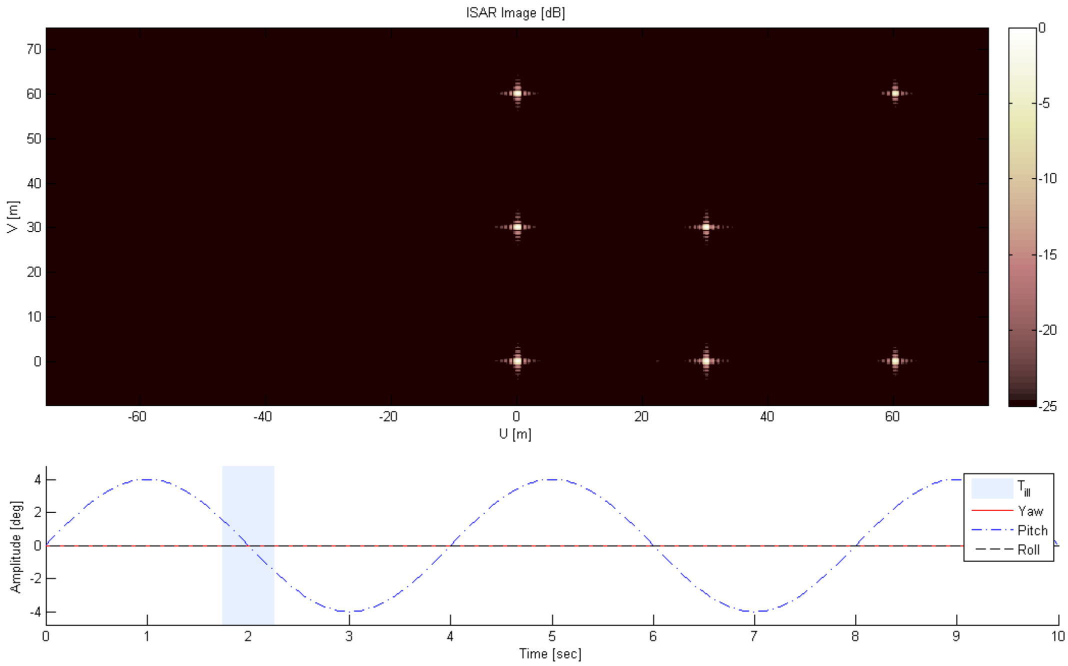

Figure 16: ISAR image in dB of seven point scatterers (upper) together with an illustration of the illuminated part of the harmonic pitch motion (lower).

3.2.1. Geometric distortion

No geometric distortion is present as could be expected from the plane wave approximation. It is a phenomenon purely based on the spherical nature of the illuminated waves.

3.2.2. Signal strength degradation

The algorithm implementation suffers from signal degradation far from the scene center. At image UV-coordinate (0,60) the signal is −0.48 dB, at (60,0) it is −1.47 dB and at (60,60) it is −2.6 dB relative the signal strength at (0,0). This problem has its origin in the interpolation in K-space. Scatterers far from the scene center stress the interpolator since they are getting closer to the allowed scene extent, determined by the sample spacing in K-space. A short test showed that linear interpolation (instead of cubic) degraded the signal even further – close to −5dB at (60, 60) relative the signal strength at (0,0). Note that the difference in U and V extent is partly due to the different sample spacing in range and cross-range[4].

3.2.3. Resolution

With equations from section 2.1.1 and an illuminated pitch angle extent of 3.06° from Figure 16, the theoretical resolution for this specific simulation can be calculated. The results are presented in Table 5 together with simulated results, see Figure 17 for illustration. Here it can be seen that the resolution is equal at both locations and hence there is no notable image defocus.

[4] Another contribution is that range samples have uniform input spacing while cross-range samples have non-uniform.

Table 5: Theoretical and simulated resolution at two different distances.

	Theory	Scatterer at (0,0)	Scatterer at (60,60)
Crossrange	0.88 m	0.90 ±0.025 m	0.90 ±0.025 m
Range	0.75 m	0.78 ±0.025 m	0.77 ±0.025 m

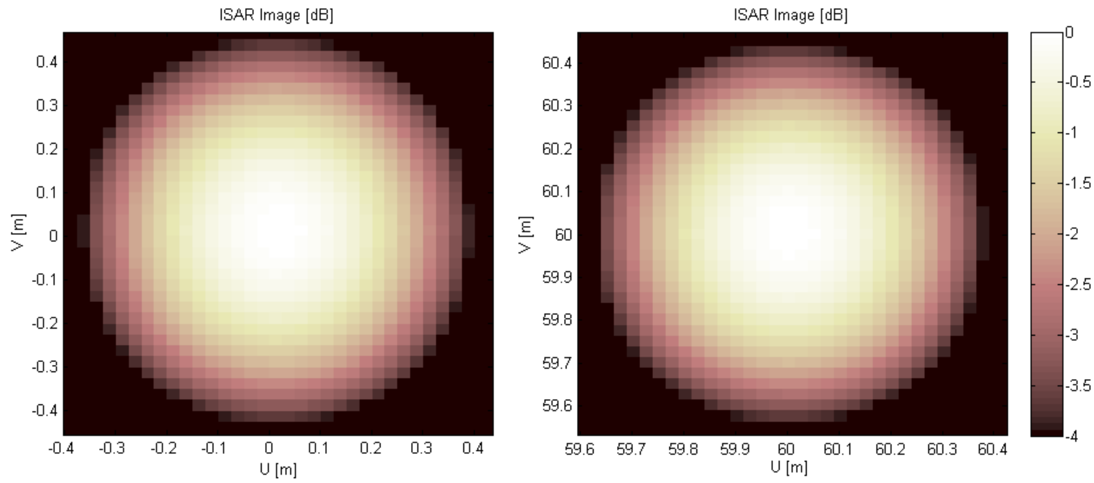

Figure 17: Response of point scatterer at origin (0,0) (left) and upper right corner (60,60) (right).

3.3. Broadside profile

One of the main reasons for using a maritime ISAR mode in an AEW&C radar platform is to enable ship type identification of tracked targets. In means of 2D ISAR images this is preferably done by classifying the ship's broadside profile. The main reason for this is that a broadside profile often provides more distinct differences between different ships than a front profile does.

Theory from section 2.1.1 with Table 1 clearly limits the ability to create broadside images to a few specific cases. The radar platform will always be at least 80 km away from the target at a height of approximately 6-7 km. To obtain best broadside resolution under these conditions, the ship should be oriented to move towards the radar platform and experience a pure pitch motion. This leads us to the first ship imaging case.

3.3.1. Pure pitch

This simulation aims to provide the best obtainable broadside image of a ship. The ship used is the model of a fishing boat and it is set to experience a pure pitch motion. Roll and yaw motions are completely absent to emphasize the pitch induced resolution. The ship is also oriented to navigate towards the radar. The simulation specific parameters are given below and the reader is referred to Section 3.1 and Table 4 for a full parametric list.

$A_y = 0$
$A_r = 0$

Resulting image and illustration of the illuminated part of the harmonic motion can be seen in Figure 18. Note that the radar illumination is occurring at a time of almost linear rotation and therefore maximum $\Delta\theta$. The image formation also assumes perfect motion knowledge and target type recognition is definitely possible under these simplified conditions. Further on, the signal strength is normalized to be 0dB for the peak value. This kind of normalization will be present in all the following images.

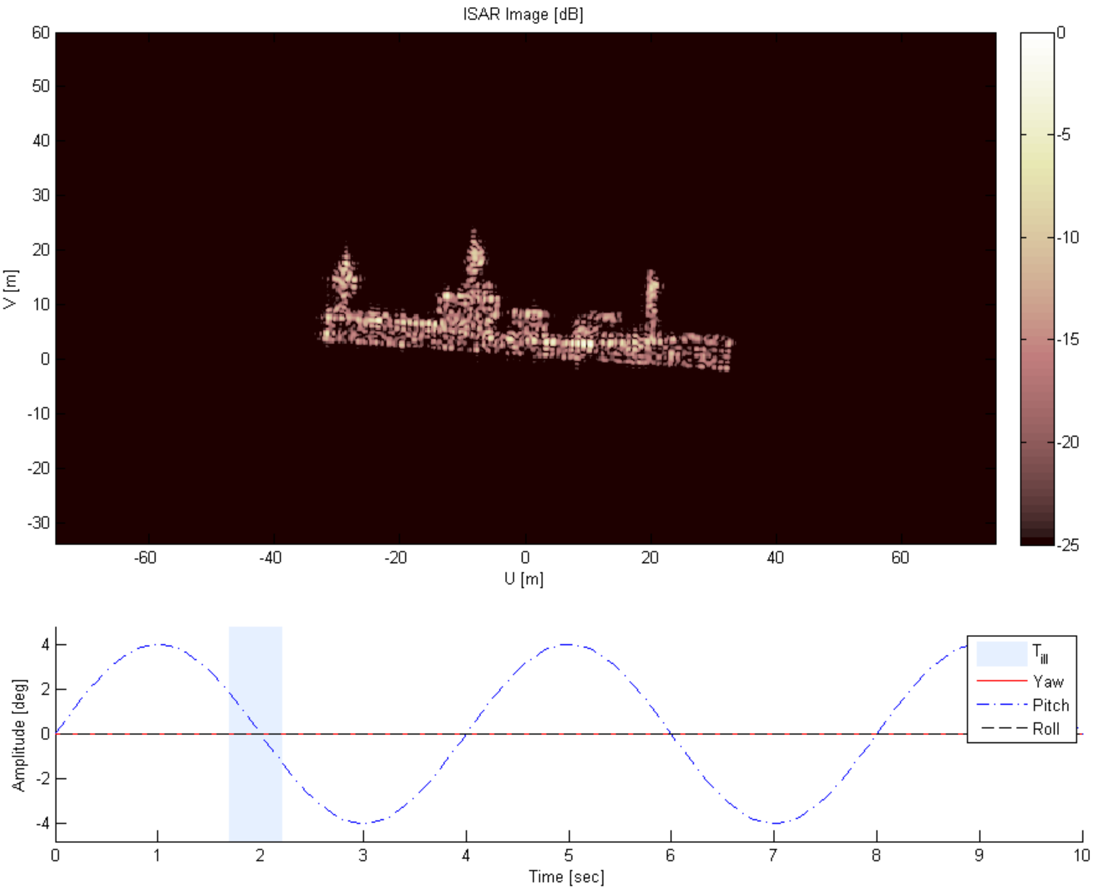

Figure 18: Best case image of a fishing boat with pure pitch motion and broadside profile. The blue-shaded area represent the coherent processing time T_{ill}. Full knowledge of the ship motion is assumed.

The non-shadowing model applied on the radar signal collection will affect signal strength distribution in the final image. Since the imaging process corresponds to a projection of the 3D-model onto the 2D IDP, bright areas will appear in the images corresponding to structures distributed perpendicular to the IDP. This can to some extent be seen in Figure 18 at the top of the hull and edges of the towers. It is good to keep this in mind when analysing simulations to come.

It is also of interest to investigate the image quality if the radar illumination happens to take place close to a minima or maxima in the harmonic pitch. This will decrease $\Delta\theta$ significantly and hence provide coarser resolution. The resulting image can be seen in Figure 19. Here the resolution is so coarse that recognition is extremely difficult.

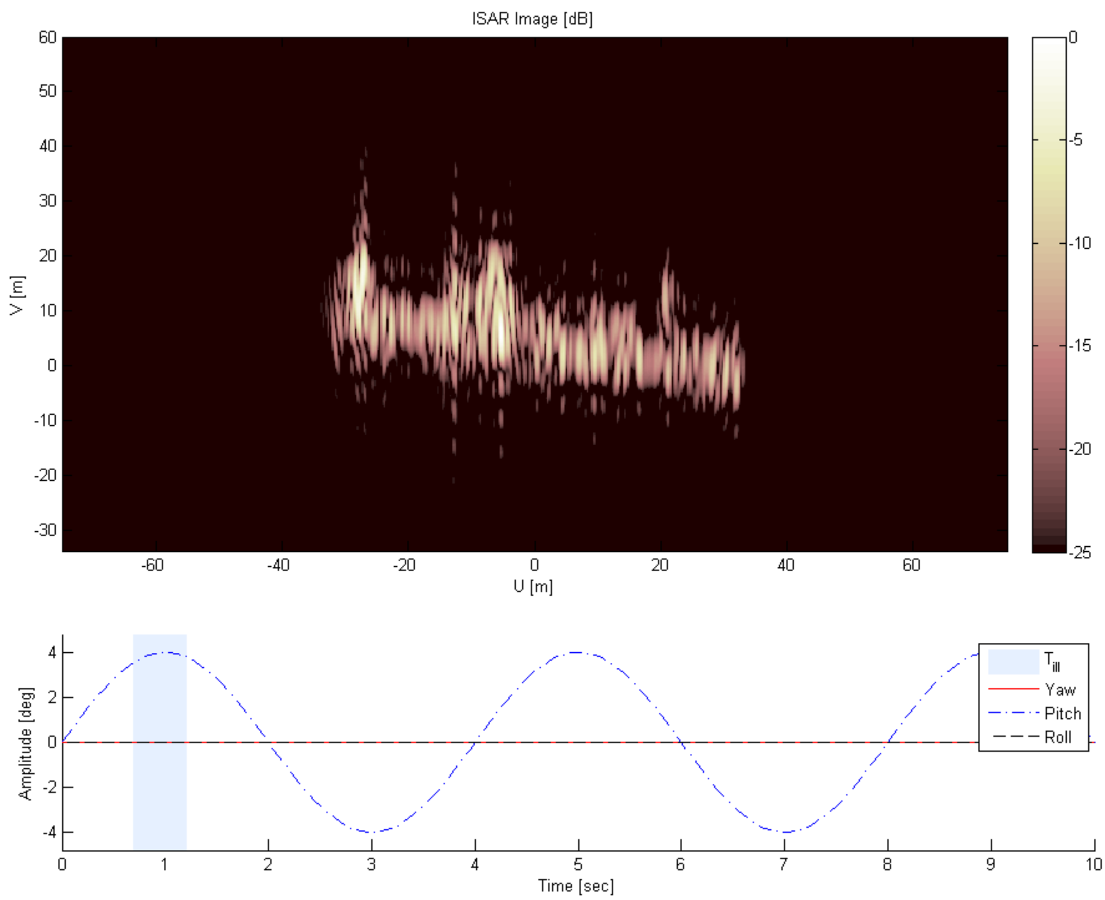

Figure 19: Worst case image of a fishing boat with pure pitch motion and broadside profile. Full knowledge of the ship motion is assumed.

3.3.2. Motion in three degrees of freedom

Section 3.3.1 provided images from a pure pitch motion case. It is now time to investigate image quality if realistic yaw- and roll motions are added. The fishing boat is still assumed to translate towards the radar and motion parameters are set according to Table 4 under the column "fishing boat". Results are showed in Figure 20 and the broadside image is slightly degraded in quality with some sidelobe increment. Target type recognition is still possible, remembering that this is under the assumption of perfect motion knowledge.

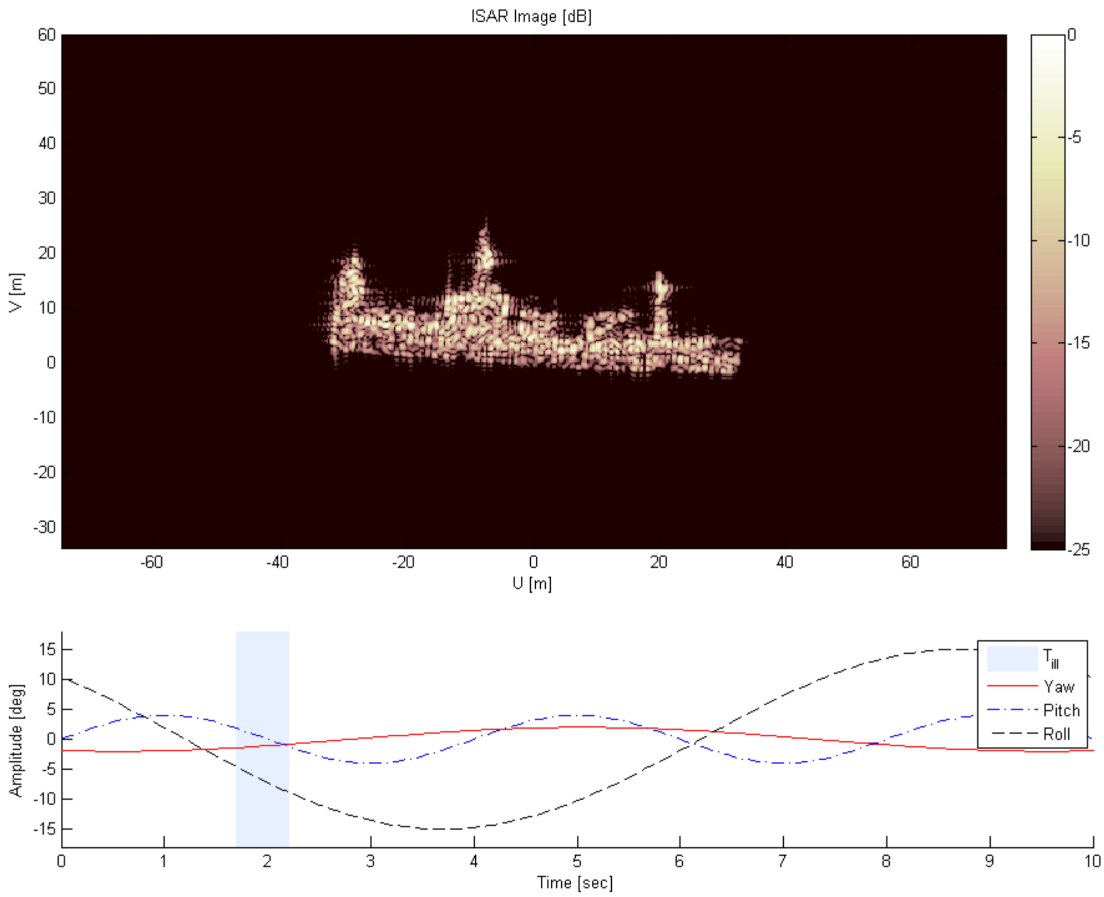

Figure 20: Best case image of a fishing boat with motion in three dimensions and broadside profile. Full knowledge of the movement is assumed.

3.4. *Dynamic IDP*

Preceding simulations have all assumed the target to be oriented to move towards the radar. If this is not the case, a fixed broadside IDP will produce coarser resolution and geometric distortion as the squint angle θ_a increases. This comes from the fact that the apparent radar vector traces an arc significantly displaced from the IDP plane. Simulations have been done for a fixed broadside IDP and a squint angle sweep θ_a = 0-90° to see at what point the target start to be unrecognizable. The results were highly dependent on the exact radar illumination instant, as well as the relative period offsets of the yaw, pitch and roll. Images are not presented here to ease readability, but a conclusion was made that at θ_a≈25-35 problems occur in identifying the ship type. Clearly, the IDP can not be fixed as the target course turns away from the radar.

To achieve highest possible vertical resolution the choice of IDP has to be dynamic, and in terms of the plane's normal vector it has to follow the squint angle θ_a with an offset of 90°. This is all in analogy with theory from section 2.1.1. A dynamic IDP simulation was therefore performed with the destroyer as target model and with two degree steps in the squint angle interval θ_a=0-90°. Images are presented for squint angles 30°, 60° and 80° in Figure 21 and Figure 22. Note that the illumination instant and motion period offsets are set to produce as high quality pictures as possible.

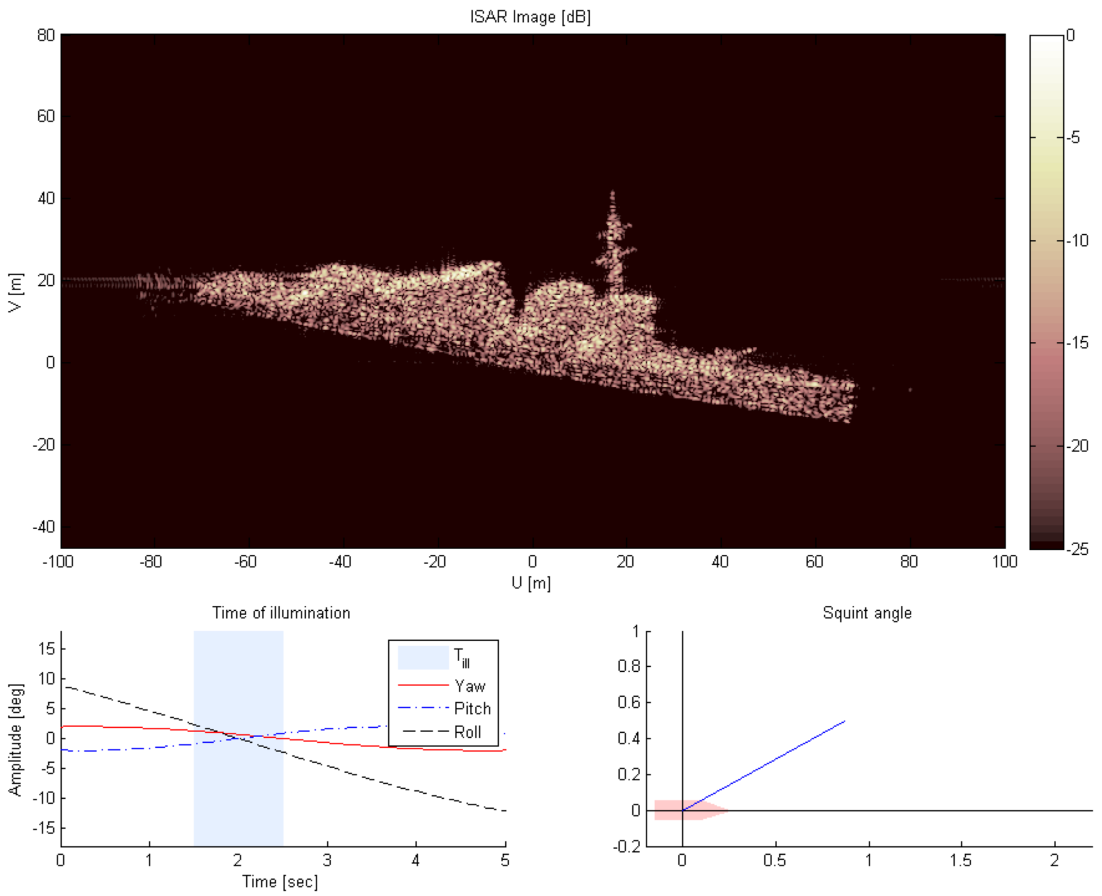

Figure 21: Image of a destroyer produced with three dimensional motion and a squint angle θ_a=30°. The IDP changes with squint angle to give best possible resolution in cross-range (IDP normal vector is offset by 90° from θ_a). Full knowledge of the ship motion is assumed.

Since motion exists in all three degrees of freedom there will be resolution in three dimensions as a result. Frequency also adds resolution, which is more stable since it is determined by the radar mode. All three presented images therefore depict the ship with a sense of it being three-dimensional.

For θ_a=30° (Figure 21) the image can still easily be identified from its broadside characteristics. At θ_a=60° (upper part in Figure 22) the ship length starts to be undeterminable but major design features, both broadside and front, are still distinct. When the squint angle gets even closer to produce front profile resolution (lower part in Figure 22), only a few type-fixed features are visible; the most dominant being the mast. Since length resolution is determined by bandwidth and height by angular motion, the depicted mast height and characteristics are extremely dependent on motion estimation when collecting the signal. In this case, full knowledge of the ship motion is assumed and the mast is therefore in it's correct scale and proportions.

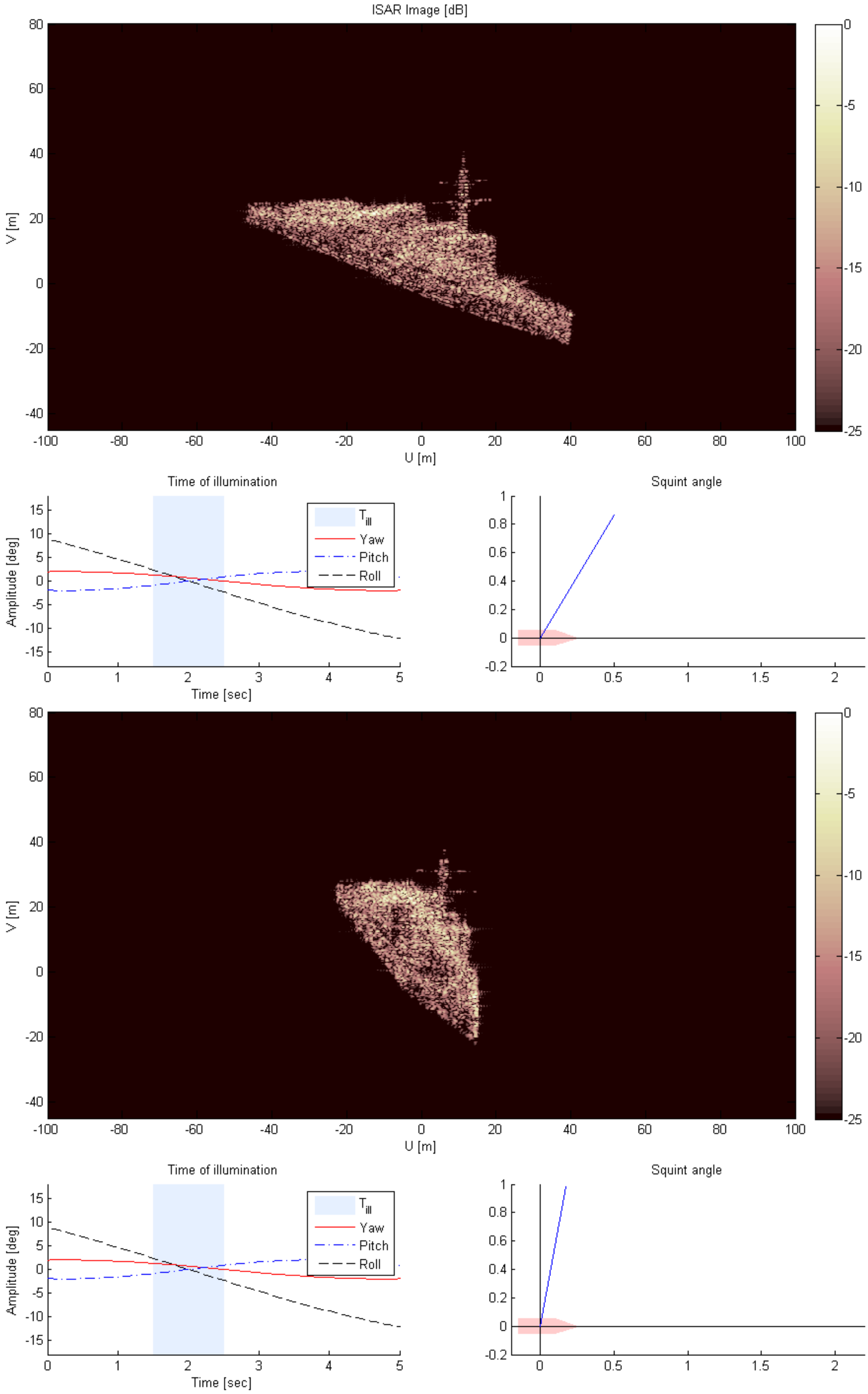

Figure 22: Image of a destroyer produced with three dimensional motion and a squint angle θ_a=60°(upper) and θ_a=80° (lower). The IDP changes with squint angle. Full knowledge of the ship motion is assumed.

3.5. Motion estimation

To make the simulations as realistic as possible an estimation regarding the ship motion has to be made. In this section the impact on target image quality will be investigated for a) motion estimation applied to a uniformly sampled polar grid, and b) a two-dimensional FFT of the collected rectangular signal matrix. Both these K-space geometries are illustrated in Figure 23.

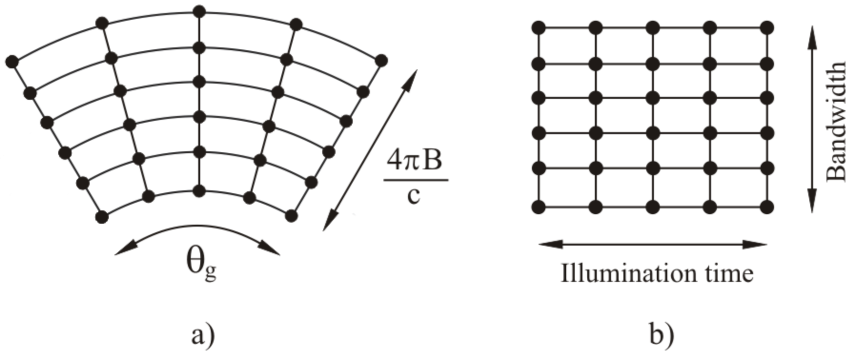

Figure 23: Signal collection grid in K-space with a) uniformly sampled polar grid with estimated angular displacement θ_g and b) collected signal matrix as rectangular grid.

The idea in a) is to estimate the maximum positive angular displacement of the target during the CPT. For a ship oriented to move towards the radar the dominant contributor to cross-range resolution would be the pitch (see Section 2.1.1 and Table 1), but in other situations it might be a complex combination of all three angular motions. Figure 24 illustrates this estimation under the assumption of a dominant harmonic motion in one degree of freedom. In case b) no estimation is necessary since it simply consist of a two-dimensional Fourier transform applied directly to the collected signal matrix.

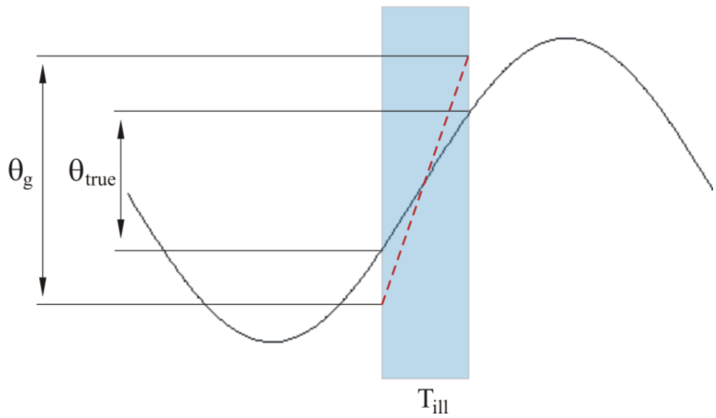

Figure 24: Estimation θ_g of total angular displacement θ_{true} during the illumination time T_{ill} for a harmonic motion in one degree of freedom.

Results are presented for imaging of the destroyer as it navigates towards the radar giving a squint angle θ_a = 0°. Estimated θ_g deviates from the true angular pitch displacement with 0 % presented in Figure 25, +50 % (upper) and −50 % (lower) in Figure 26. The result of the two-dimensional FFT of the collected signal matrix is presented in Figure 27. Actual simulations have been done for 65 different CPT instants in the presented time interval in each figure. Images are merely presented from one illumination instant, with relatively good motion for depicting the target, remembering that other more misfortunate instants would result in poorer image quality. This choice is made to ease readability and conclusions.

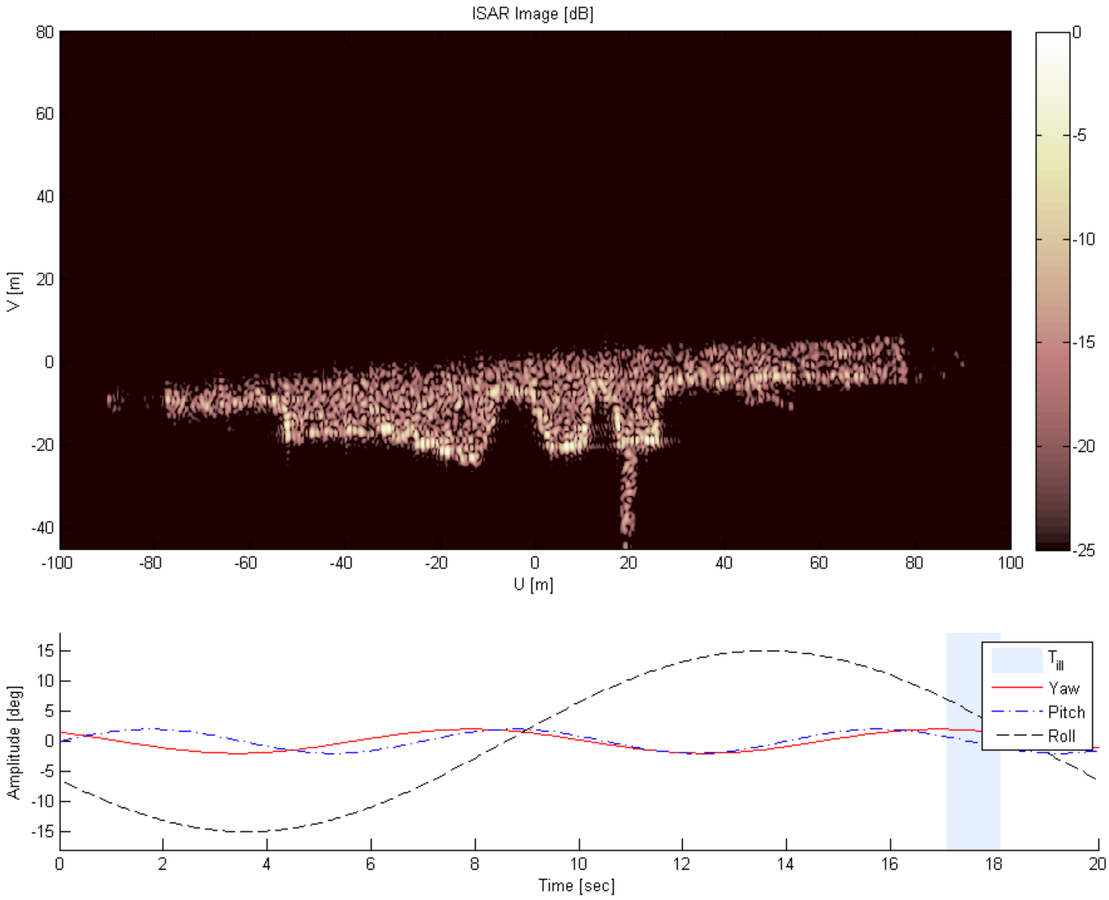

Figure 25: Image of destroyer with θ_a=0°, three dimensional motion and 0% deviation in gradient guess.

In Figure 25 to Figure 27 the ship appear to be upside down. This instant is chosen with the intention to display effects that can occur in real life scenarios. The reason for the ship appearing to be upside down is quite easily understood when you look at the characteristics of the pitch motion during the CPT and how the estimated gradient is oriented. Doing this comparison you can see that the actual movement and the estimated one have the complete opposite direction, resulting in an upside down image. During the different CPT instants mentioned above both upside down and correctly oriented images will occur.

Figure 26 shows the simulated results for an estimated gradient that have +50 % and −50 % deviations from the correct angular displacement. This means that the estimated θ_g is equal to $1.5 \cdot \theta_{true}$ and $0.5 \cdot \theta_{true}$ respectively, resulting in a deformation of the final image. For a gradient that deviates by +50 % the angular extent is increased in the collection grid in K-space. This increment results in sparser cross-range sampling since the number of samples is still the same. Theory from section 2.1.4 states that scene extent is inversely related to sample spacing, which in this case leads to a smaller scene extent and thereby a compressed image. The exact opposite occurs when the gradient deviates by −50 % and the image seems to be stretched out in cross-range.

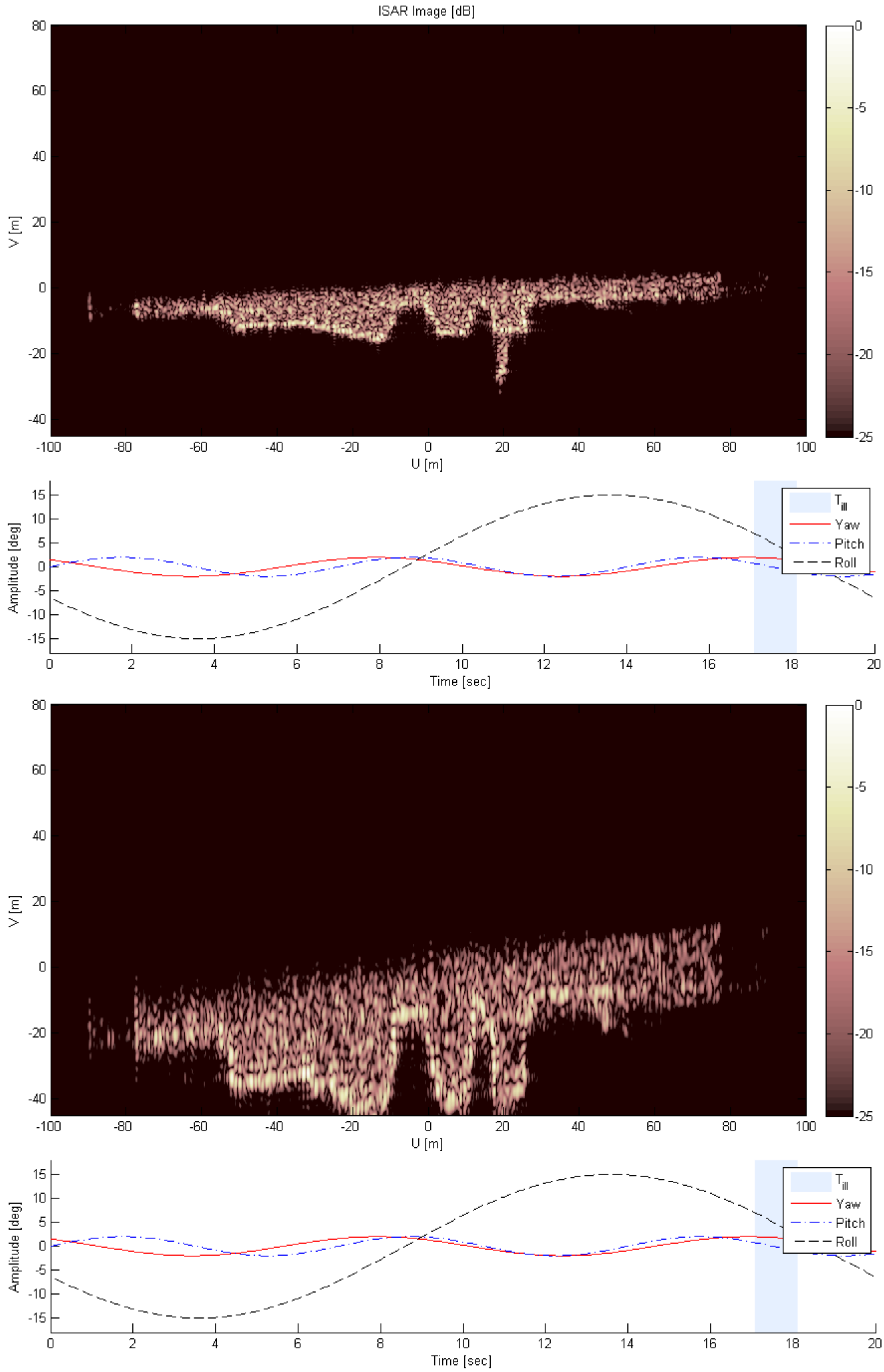

Figure 26: Image of destroyer with θ_a=0°, three dimensional motion and +50 % deviation in gradient guess for the above picture and -50 % deviation for the one below. The lower image is not fully shown due to the zooming window chosen for creating satisfactory movie frames. The ship is within the scene extent limits.

Figure 27 shows the corresponding picture for the use of a rectangular grid resulting from applying a two-dimensional FFT directly on the collected signal, see Figure 23b). Here you can see that the resolution is a bit coarser than in the corresponding estimated images above and take note of the change in axes. The metric cross-range distance has been replaced with a measure in Doppler frequency. Image quality from this procedure was found to be more than sufficient for identification in relation to its complexity. The reason for this is the small angular displacement during the CPT and the high carrier frequency, resulting in a true collection geometry which is close to a rectangular grid in K-space – see Figure 28.

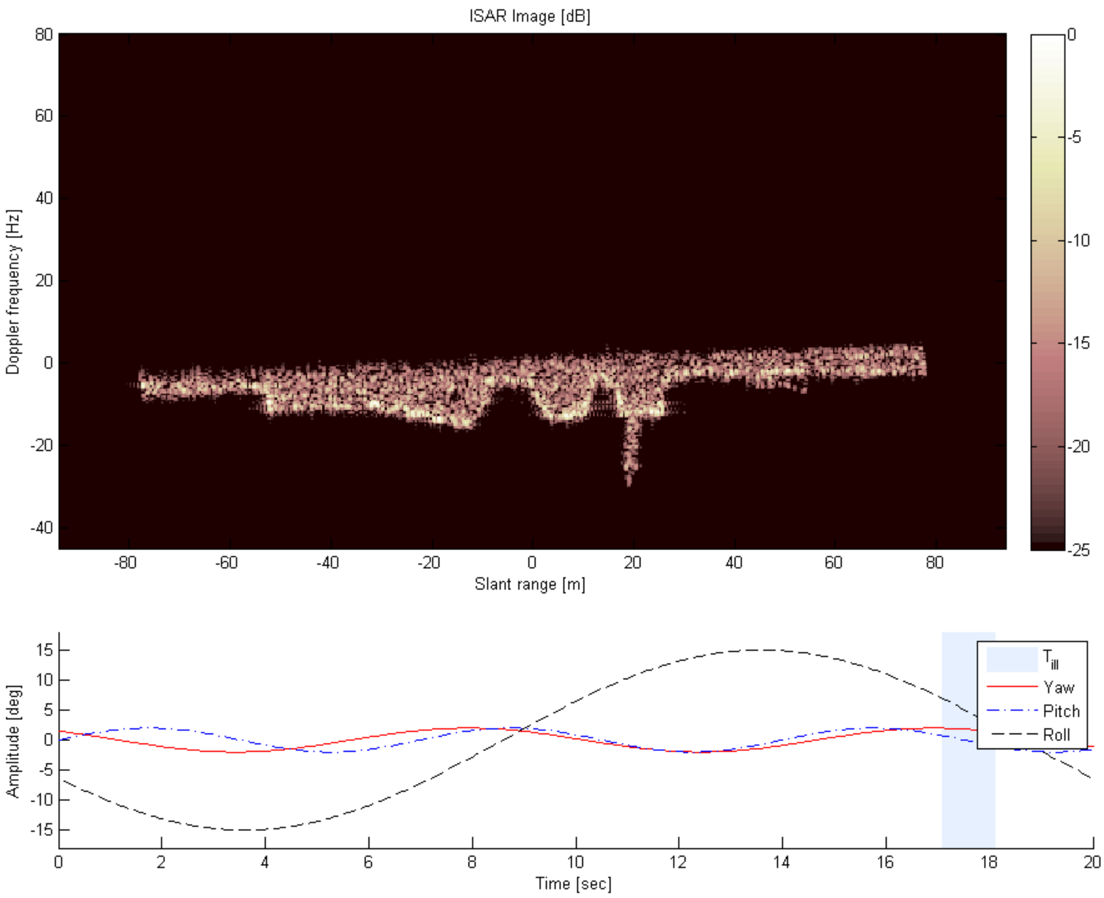

Figure 27: Image of destroyer with θ_a=0°, three dimensional motion and two-dimensional FFT applied directly to the collected rectangular signal matrix.

The simulations are, as mentioned before, performed with 65 different illuminations covering the presented time interval in each figure. Each CPT started 0.3 s later then the proceeding one, allowing the creation of movies with slight interlays between nearest frames. These movies were then used to show the dynamic image quality from instant to instant and also to observe the most interesting result – how often the ship type can be identified.

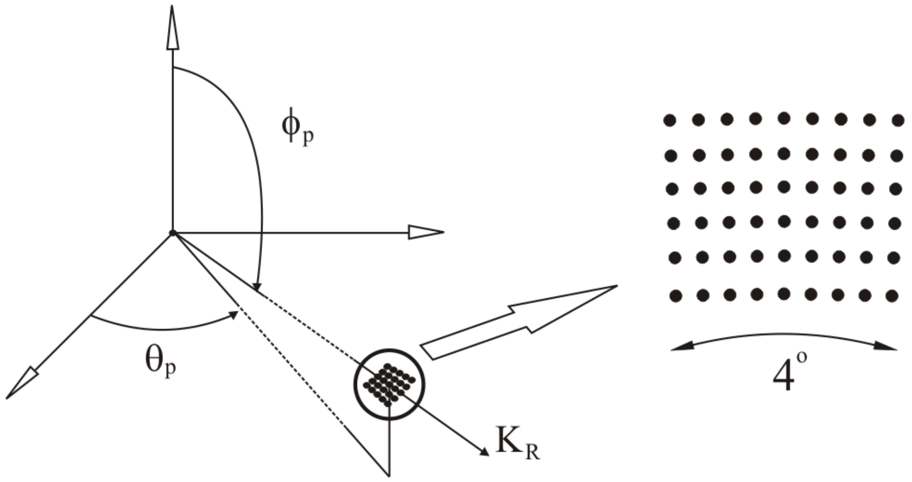

Figure 28: Illustration of the collection geometry for a small angle of 4 degrees. Here it can be seen that the collection grid is close to rectangular.

To be able to asses how valuable the simulated results are, a table has been developed indicating how often the images are of such quality that they can be used for identification, see Table 6. Here it can be seen that about 60 % of the images have a quality that corresponds to being able to identify the target. This table has been created from qualitative ratings by the authors based on the ability to distinguish major design features such as towers, masts and size. The rating is highly dependent on the operator and therefore only given for guidance purpose and attached with a 5 % safety margin.

Table 6: Number of frames in percent that can be used to identify the destroyer.

Case	**Percentage (±5 %)**
Gradient estimation with 0 % deviation	60 %
Gradient estimation with +50 % deviation	60 %
Gradient estimation with −50 % deviation	60 %
FFT of collected signal matrix	65 %

From these investigations one can see that using an estimated gradient during the CPT seems to give equivalent results as for using a two-dimensional FFT on the collected signal matrix. Significant errors in the gradient guess also seem to give valuable results.

3.6. Changes in coherent processing time

Authors of [16] lay emphasize on the choice of a suitable CPT for ISAR imaging of cooperative sea vessels. This choice is highly dependent on the target motion and this section assumes amplitude and period parameters for the destroyer to investigate its importance. Based on our own observations from preceding results, together with information from [16], three reasonable values have been investigated: T_{ill} = 0.5, 1 and 2 s. These values are relevant for imaging larger ships, such as the destroyer. The squint angle has been set to θ_a=45° to simulate a scenario were all motions contribute to resolution.

To highlight the influence of T_{ill} on image quality the assumption of perfect motion knowledge has been used. Effects from motion estimation etc. are therefore not present in this simulation. First the middle value T_{ill} = 1 s is presented in Figure 29 followed by both T_{ill} = 0.5 s (upper) and T_{ill} = 2 s (lower) in Figure 30.

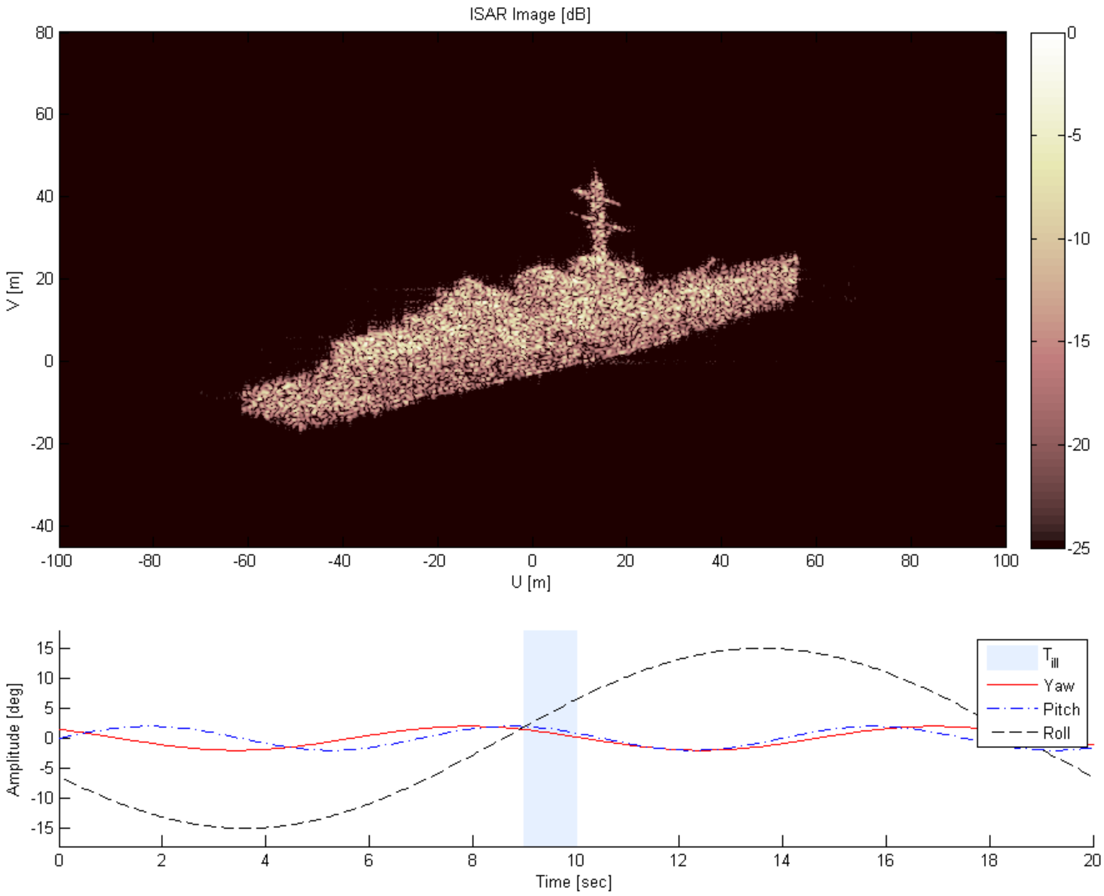

Figure 29: Image of destroyer with θ_a=45°, dynamic IDP and T_{ill} = 1 sec.

All three values of the CPT provide sufficient resolution to identify the destroyer during a favorable motion instant. Before the more detailed discussion continues it is worth noting that the distortion in the lower part of Figure 30 comes from problems in the interpolation step.

After looking at all three images it is clear that a longer CPT results in a wider coherent angular interval, and hence finer resolution. This is actually straight forward when the motion instant is favorable. The situation gets a bit more complex if the resolution contributing motion is in its periodic end-position. Then the phase information is more or less the same before and after the peak value and resolution gets coarser[5]. For typical rotational periods of a large ship this will actually work in favor of lower values of T_{ill}.

[5] The information is not identically the same since the other two angular motions are changing and hence destroys the equivalence. Assessing the contributing extent of this phenomenon is beyond the scope of this master thesis.

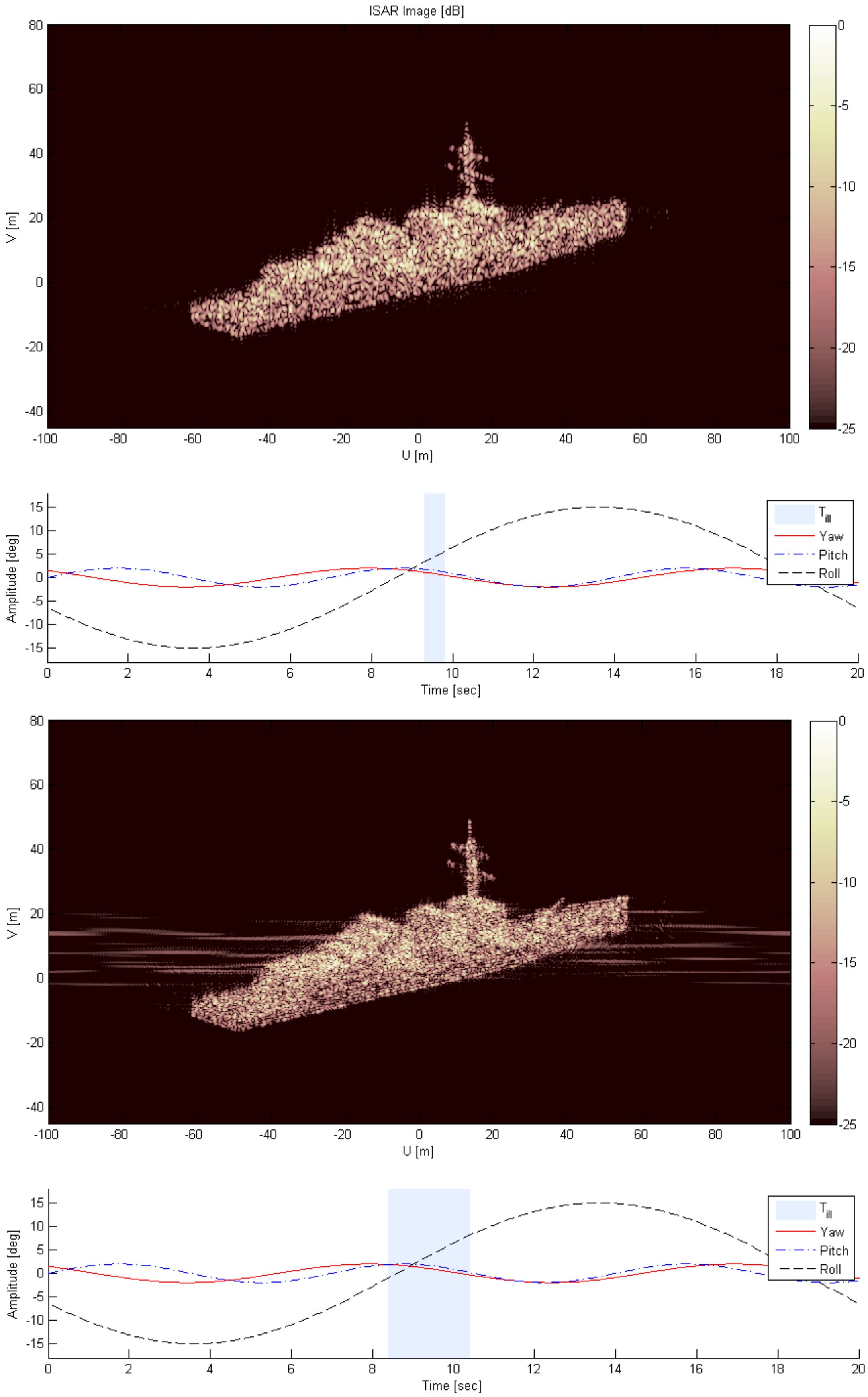

Figure 30: Image of destroyer with θ_a=45° and dynamic IDP. Upper image uses a CPT of T_{ill} = 0.5 s and the lower image uses T_{ill} = 2 s.

As in section 3.5 movies were created to show the dynamic image quality from instant to instant and also to observe the most interesting result – how often the ship type can be identified.

Table 7 presents a percentage of the number of frames that are possible to do type identification from. Both the case of perfect motion knowledge and the case of no knowledge have best results for a CPT of 1 s. The values deviates quite considerably compared to the ones displayed in Table 6. This is to be expected since the first simulation uses θ_a=0° and the second θ_a=45°, which leads to less accentuated broadside characteristics in the latter.

Table 7: Number of frames in percent that can be used to identify the destroyer.

Case		Percentage (±5 %)
Till = 0.5 s	Perfect motion knowledge	35 %
Till = 1 s	Perfect motion knowledge	50 %
Till = 2 s	Perfect motion knowledge	40 %
Till = 0.5 s	FFT of collected signal matrix	25 %
Till = 1 s	FFT of collected signal matrix	35 %
Till = 2 s	FFT of collected signal matrix	30 %

It was some discussion above about having the CPT centered on the peak angular displacement in the ship's harmonic motion. The collection geometry applied while having perfect motion knowledge then experience degraded resolution. If the angular displacement returns to a preceding value the apparent radar vector will trace the same position in K-space again. Figure 31 illustrate the mirroring phenomenon that arises when directly processing the collected signal matrix. This collection geometry is rectangular and continues with uniform sample spacing over time, regardless of CPT position. If the angular displacement is both increasing and decreasing during the CPT, the depicting will experience cross-range mirroring effects as in Figure 31.

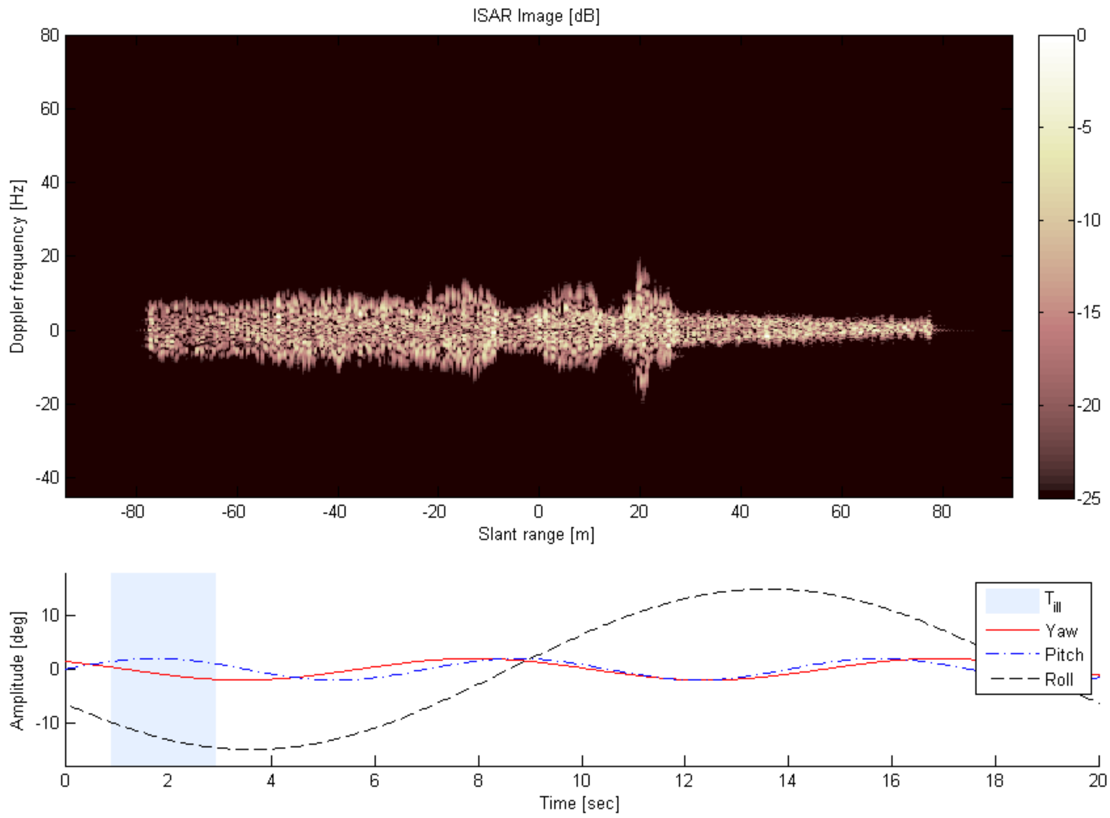

Figure 31: Image of destroyer with θ_a=0°, T_{ill} = 2 s and FFT processing of the collected signal matrix. A mirroring effect is present during this processing technique due to the CPT being centered on the peak angular displacement of the pitch motion.

3.7. Decreased roll motion

This section addresses the uncertainty in roll amplitude and what effects to be expected from lower roll displacements. Theory in section 2.2.1 stated that roll amplitudes in sea state 4 may be single digit degrees for certain roll suppressing designs. It is however varying quite considerable from ship to ship which makes it difficult to estimate. So far the roll amplitude has been set to 15°, which is rather high but in the span of reality. It is therefore wise to supplement with an example based on lower roll amplitude.

Figure 32 illustrate image quality with roll angle amplitude of 7.5° instead of the preceding 15°. The squint angle has been set to 45° to provide a situation where roll motion actually contributes to resolution to roughly the same extent as the pitch does. Some sidelobe increment and degradation in resolution is notable, but the image is still good enough to use for type identification.

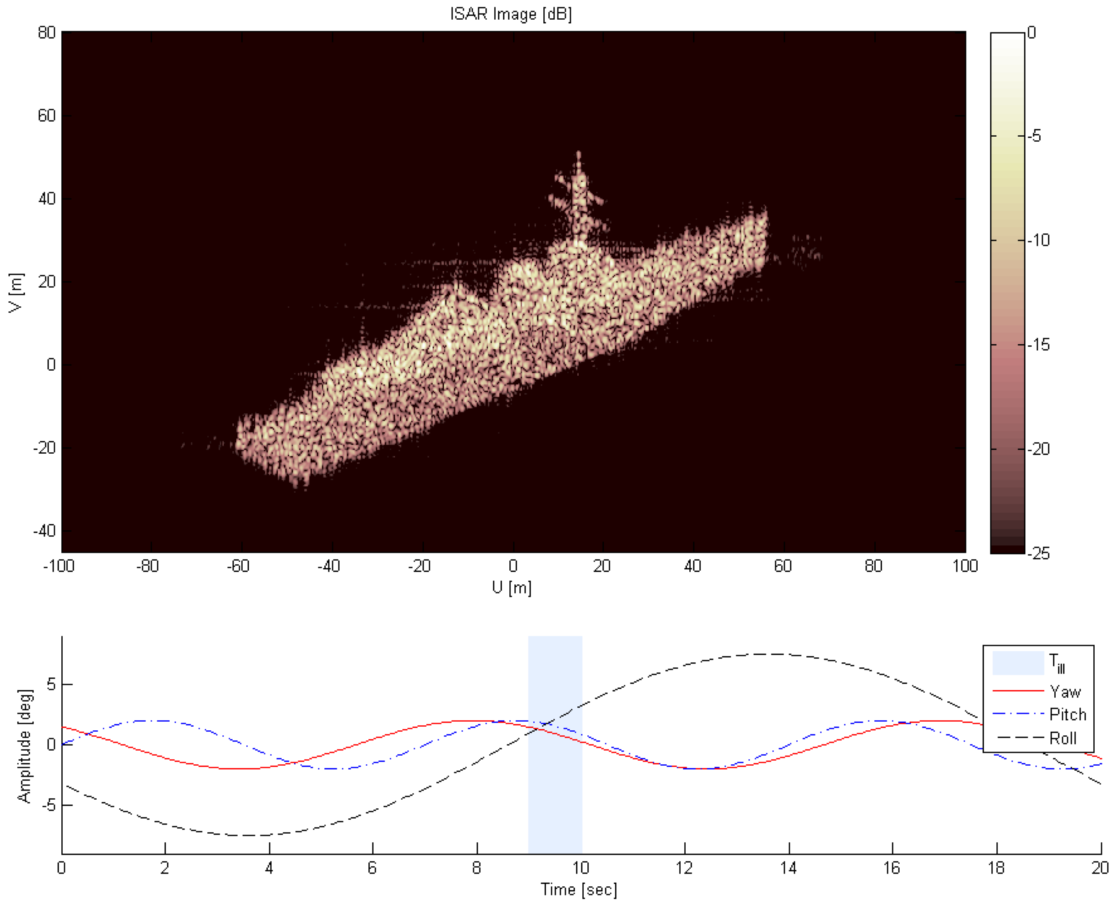

Figure 32: Image of destroyer with θ_a=45°, T_{ill} = 1 s and A_r=7.5°.

4. Conclusions

The overall impression of using ISAR for depicting maritime targets is so far to our satisfaction. However, too much is left unexplored to make a definitive decision about implementing it in an airborne radar platform. One example is how well our 3D ship models, consisting of point scatterers, actually represent reality. More specifically there is great uncertainty and little knowledge regarding RCS fluctuations for different parts of the ship as well as RCS fluctuations over time. The final image could be deformed beyond recognition if the phase responses vary too much between time samples.

Another important aspect of the physical modeling is the realized motion. We chose to use three of the six oscillatory motions, modeled with pure harmonic equations, mainly since it was sufficient in relation to the aim of our thesis. The effects of the remaining three (surge, sway and heave) are generally considered to have a minor impact on the imaging process. There is however an uncertainty regarding deviations from the harmonic model and its impact on image quality. For example, the author of [13] presents measured values of yaw motion, showing some noise-like behavior that could be of importance. Authors of [16] present measured values for bank, elevation and heading for cooperative sea vessel which also show similar behavior.

Looking beyond these limitation one can still make several interesting observations. To start with, a dynamic IDP should be used in advanced collecting geometries and its normal vector should follow the squint angle with an offset of 90°. This has been motivated by both theory and simulations. It has also been shown that the modeled ship motion provide sufficient resolution for type identification. The most uncertain parameter here was the roll amplitude, which showed to have minor effect on image quality when lowered significantly.

The next major part of the simulations dealt with unknown motion and estimation of it. A polar grid estimation technique was tested with a 50 % error in the estimated angular displacement. Results were still possible to use for target identification. These estimations were then compared with a direct Fourier processing of the collected signal matrix with rather unexpected results. The simplest possible algorithm still provided images of sufficient quality and could therefore be used in an initial testing stage.

Inspired by [16] we also did an assessment regarding the choice of coherent processing time. The initial idea of a CPT around one second for larger ships proved to be in the right order of magnitude. Amplitude and period of the resolution contributing motion seems to be of great importance. Smaller ships often has larger pitch and roll motions, which further indicates that the CPT could be reduced to as low as half a second and still provide satisfying image quality.

Worth mentioning is also some additional possible contributors to image degradation in an operational system, such as hardware limitations and clutter. One could expect a significant lowering of the amount of usable images if these effects are not coped with.

Lastly we would like to point out that a crucial step in future algorithm development might be the interpolation step. The problem arises in the transition between a non-uniform and non-monotonic input grid to a uniform output grid.

5. Future work

Maritime ISAR shows great potential in depicting naval targets. Below is a list of suggestions on how to continue the work presented in this report.

- Further investigate the possibility of using simple algorithms such as the direct Fourier processing of the collected signal.
- Perform field study of RCS fluctuation over time/angle for different ships by measuring the ships' instantaneous RCS values.
- Perform field trial with an electronically steered array and process the signal with an ISAR algorithm.
- Investigate the advantages of introducing an autofocus technique.

Acknowledgements

The authors are grateful to:

- Saab EDS at Kallebäck, Gothenburg, for giving us the opportunity to work with this interesting subject and for great support during the process.
- Special thanks to our supervisor at Saab EDS, Björn Hallberg, for his patience and guidance throughout this master thesis work.
- Lars Ulander at Chalmers University of Technology for help with the revision of this report.
- Naval expert Martin Schreuder at Chalmers University of Technology for interesting and rewarding deliberations regarding the subject of ship motion.
- Patrik Dammert at Saab EDS at Lackarebäck, Gothenburg, for valuable discussions and shown interest in our work.

References

[1] Walter G. Carrara, Ron S. Goodman and Ronald M. Majewski, *"Spotlight Synthetic Aperture Radar – Signal Processing Algorithms"*, Copyright © Artech house, inc. 1995.

[2] Donald R. Wehner, *"High Resolution Radar"*, 1987 © Artech house, inc. 1987.

[3] G. Hajduch, J.M. Le Caillec, R. Garello, *"Airborne high-resolution ISAR imaging of ship targets at sea"*, Aerospace and Electronic Systems, IEEE Transactions on , vol. 40, no. 1, pp. 378-384, Jan 2004.

[4] Y. Li, R. Wu, M. Xing, Z. Bao, *"Inverse synthetic aperture radar imaging of ship target with complex motion"*, Radar, Sonar & Navigation, IET, vol. 2, no. 6, pp. 394-403, December 2008.

[5] Z. Bao, G. Wang, L. Luo, *"Inverse synthetic aperture radar imaging of maneuvering targets"*, Opt. Eng. vol. 37, no. 5, pp. 1582-1588 , May 1998.

[6] S. Musman, D. Kerr, C. Bachmann, *"Automatic recognition of ISAR ship images"*, Aerospace and Electronic Systems, IEEE Transactions, Volume 32, Issue 4, Oct. 1996, © 1996 IEEE , pp. 1392 – 1404.

[7] B. Zheng, S. Changyin, X. Mengdao, *"Principles and algorithms for inverse synthetic aperture radar imaging of maneuvering targets"*, IEEE Radar Conference, 2000, The Record of the IEEE 2000 International, pp. 316-321, 2000.

[8] Dan Slater, *"Inverse Synthetic Aperture Imaging Radar"*, Antenna Measurement Techniques Association Conference 1985, Nearfield Systems Incorporated, TRW Military Electronics Division, Antenna Organization.

[9] J. Gao, F. Su, X. Cao, G. Xu, *"Simulation of ISAR Imaging of Ships with Multipath Effects"*, Industrial Electronics and Applications, 2007, ICIEA 2007, 2nd IEEE Conference on, pp. 1484-1488, 23-25 May 2007.

[10] C. Beaudoin, A. Gatesman, M. Clinard, J. Waldman, R. Giles and W. Nixon, *"Physical Scale Modeling of VHF/UHF SAR Collection Geometries",* Submillimeter-Wave Tchnology Laboratory, University of Massachusetts Lowel.

[11] *"MATLAB® 7, Function Reference: Volume 2 (F-O)"*, ©1984-2010 by The MathWorks Inc.

[12] Armin W. Doerry*, "Ship Dynamics for Maritime ISAR Imaging",* SAR application department, Sandia National Laboratories, Albuquerque, February 2008.

[13] Edward V. Lewis, editor Jersey City, N.J., *"Principles of naval architecture - Vol. 3, Motions in waves and controllability"*, Society of naval architects and marine engineers, 1989.

[14] MathWorld, *"Euler Angles"*, retrieved 2010-03-25, available at: http://mathworld.wolfram.com/EulerAngles.html

[15] Lennart Råde, Bertil Westergren, *"Mathematics Handbook for Science and Engineering, BETA"*, Studentlitteratur 1995.

[16] M. Y. Abdul Gaffar, W. A. J. Nel, and M. R. Inggs, *"Selecting Suitable Coherent Processing Time Window Lengths for Ground-Based ISAR Imaging of Cooperative Sea Vessels"*, IEEE Transactions on Geoscience and Remote sensing, vol. 47, no. 9, pp. 3231-3240, September 2009.